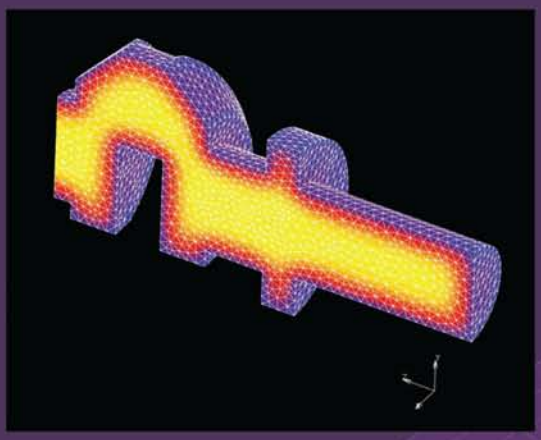

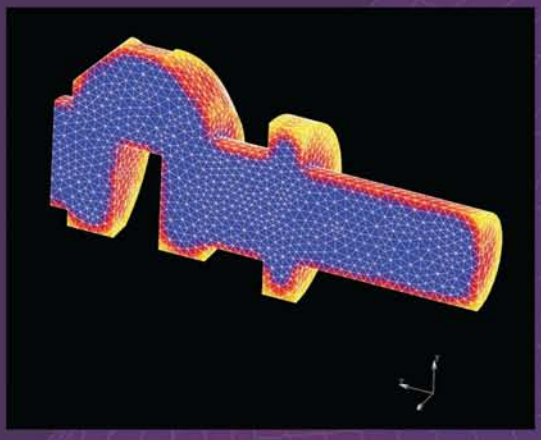

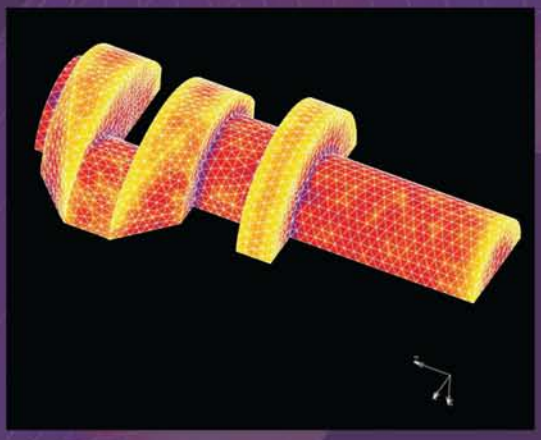

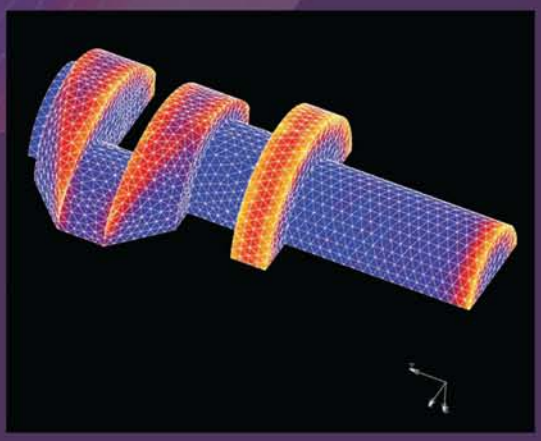

Handbook of Thermal Process Modeling of Steels

EDITED BY
CEMIL HAKAN GÜR
JIANSHENG PAN

IFHTSE
INTERNATIONAL FEDERATION FOR HEAT TREATMENT AND SURFACE ENGINEERING

CRC Press
Taylor & Francis Group

Handbook of

Thermal Process Modeling of Steels

Handbook of

Thermal Process Modeling of Steels

Edited by
Cemil Hakan Gür
Jiansheng Pan

CRC Press
Taylor & Francis Group
Boca Raton London New York

CRC Press is an imprint of the
Taylor & Francis Group, an **informa** business

IFHTSE
INTERNATIONAL FEDERATION
FOR HEAT TREATMENT AND
SURFACE ENGINEERING

CRC Press
Taylor & Francis Group
6000 Broken Sound Parkway NW, Suite 300
Boca Raton, FL 33487-2742

Printed in the United States of America on acid-free paper
10 9 8 7 6 5 4 3 2 1

International Standard Book Number-13: 978-0-8493-5019-1 (Hardcover)

Visit the Taylor & Francis Web site at
http://www.taylorandfrancis.com

and the CRC Press Web site at
http://www.crcpress.com

Contents

Preface

The whole range of steel thermal processing technology, from casting and plastic forming to welding and heat treatment, not only produces workpieces of the required shape but also optimizes the end-product microstructure. Thermal processing thus plays a central role in quality control, service life, and the ultimate reliability of engineering components, and now represents a fundamental element of any company's competitive capability.

Substantial advances in research, toward increasingly accurate prediction of the microstructure and properties of workpieces produced by thermal processing, were based on solutions of partial differential equations (PDEs) for temperature, concentration, electromagnetic properties, and stress and strain phenomena. Until the widespread use of high-performance computers, analytical solution of PDEs was the only approach to describe these parameters, and this placed severe limitations in terms of prediction for engineering applications so that thermal process developments themselves relied on empiricism and traditional practice. The level of inaccuracy inherent in computational predictions hindered both materials performance improvements and process cost reduction.

Since the 1970s, the pace of development of computer technology has made possible effective solution of PDEs in complicated calculations for boundary and initial conditions, as well as nonlinear and multiple variables. Mathematical models and computer simulation technology have developed rapidly; currently well-established mathematical models integrate fundamental theories of materials science and engineering including heat transfer, thermoelastoplastic mechanics, fluid mechanics, and chemistry to describe physical phenomena occurring during thermal processing. Further, evolution of transient temperature, stress–strain, concentration, microstructure, and flow can now be vividly displayed through the latest visual technology, which can show the effects of individual process parameters. Computation/simulation thus provides an additional decision-making tool for both the process optimization and the design of plant and equipment; it accelerates thermal processing technology development on a scientifically sound computational basis.

The basic mathematical models for thermal processing simulation gradually introduced to date have yielded enormous advantages for some engineering applications. Continued research in this direction attracts increasing attention now that the cutting-edge potential of future developments is evident. Increasingly profound investigations are now in train globally. The number of important research papers in the field has risen sharply over the last three decades. Even so, the existing models are regarded as highly simplified by comparison with real commercial thermal processes. This has meant that the application of computer simulation has thus far been relatively limited precisely because of these simplifying assumptions, and their consequent limited computational accuracy. Extensive and continuing research is still needed.

This book is now offered as both a contribution to work on the limitations described above and as an encouragement to increase the understanding and use of thermal process models and simulation techniques.

The main objectives of this book are, therefore, to provide a useful resource for thermal processing of steels by drawing together

- An approach to a fundamental understanding of thermal process modeling
- A guide to process optimization
- An aid to understand real-time process control
- Some insights into the physical origin of some aspects of materials behavior
- What is involved in predicting material response under real industrial conditions not easily reproduced in the laboratory

Linked objectives are to provide

- A summary of the current state of the art by introducing mathematical modeling methodology actually used in thermal processing
- A practical reference (industrial examples and necessary precautionary measures are included)

It is hoped that this book will

- Increase the potential use of computer simulation by engineers and technicians engaged in thermal processing currently and in the future
- Highlight problems requiring further research and be helpful in promoting thermal process research and applications

This project was realized due to the hard work of many people. We express our warm appreciation to the authors of the respective chapters for their diligence and contribution. The editors are truly indebted to everyone for their contribution, assistance, encouragement, and constructive criticism throughout the preparation of this book.

Here, we also extend our sincere gratitude to Dr. George E. Totten (Totten Associates and a former president of the International Federation for Heat Treatment and Surface Engineering [IFHTSE]) and Robert Wood (secretary general, IFHTSE), whose initial encouragement made this book possible, and to the staff of CRC Press and Taylor & Francis for their patience and assistance throughout the production process.

C. Hakan Gür
Middle East Technical University

Jiansheng Pan
Shanghai, Jiao Tong University

Editors

C. Hakan Gür is a professor in the Department of Metallurgical and Materials Engineering at Middle East Technical University, Ankara, Turkey. He is also the director of the Welding Technology and Nondestructive Testing Research and Application Center at the same university. Professor Gür has published numerous papers on a wide range of topics in materials science and engineering and serves on the editorial boards of national and international journals. His current research includes simulation of tempering and severe plastic deformation processes, nondestructive evaluation of residual stresses, and microstructures obtained by various manufacturing processes.

Jiansheng Pan is a professor in the School of Materials Science and Engineering at Shanghai Jiao Tong University, Shanghai, China. He was an elected member of the Chinese Academy of Engineering in 2001. Professor Pan's expertise is in chemical and thermal processing of steels (including nitriding, carburizing, and quenching) and their computer modeling and simulation. He has established mathematical models of these processes integrating heat and mass transfer, continuum mechanics, fluid mechanics, numerical analysis, and software engineering. These models have been used for computational simulation to design and optimize thermal processes for parts with complicated shape. Pan and his coworkers have published extensively in these areas and have been awarded over 40 Chinese patents. In addition to a number of awards for scientific and technological achievements, Professor Pan was the president of the Chinese Heat Treatment Society (2003–2007) and is the chairman of the Mathematical Modeling and Computer Simulation Activity Group of the International Federation for Heat Treatment and Surface Engineering.

Contributors

María Victoria Bongiovanni
Facultad de Ingeniería
Universidad Austral
Buenos Aires, Argentina

and

Facultad de Ciencias Exactas y Naturales
Universidad de Buenos Aires
Buenos Aires, Argentina

Chris H.J. Davies
Department of Materials Engineering
Monash University
Melbourne, Victoria, Australia

Janez Grum
Faculty of Mechanical Engineering
University of Ljubljana
Ljubljana, Slovenia

Jianfeng Gu
School of Materials Science and Engineering
Shanghai Jiao Tong University
Shanghai, China

C. Hakan Gür
Department of Metallurgical and Materials Engineering
Middle East Technical University
Ankara, Turkey

Sivaraman Guruswamy
Department of Metallurgical Engineering
University of Utah
Salt Lake City, Utah

Bernardo Hernandez-Morales
Departamento de Ingeniería Metalúrgica
Universidad Nacional Autónoma de México
Mexico

Peter Hodgson
Centre for Material and Fibre Innovation
Institute for Technology Research and Innovation
Deakin University
Geelong, Victoria, Australia

John J. Jonas
Department of Materials Engineering
McGill University
Montreal, Quebec, Canada

Valentin Nemkov
Fluxtrol, Inc.
Auburn Hills, Michigan

and

Centre for Induction Technology
Auburn Hills, Michigan

Jiansheng Pan
School of Materials Science and Engineering
Shanghai Jiao Tong University
Shanghai, China

Mario Rosso
R&D Materials and Technologies
Politecnico di Torino
Dipartimento di Scienza dei Materiali e Ingegneria Chimica
Torino, Italy

and

Politecnico di Torino
Sede di Alessandria
Alessandria, Italy

Satyam Suraj Sahay
Tata Research Development and Design Centre
Tata Consultancy Services Limited
Pune, Maharashtra, India

Gustavo Sánchez Sarmiento
Facultad de Ingeniería
Universidad de Buenos Aires
Buenos Aires, Argentina

and

Facultad de Ingeniería
Universidad Austral
Buenos Aires, Argentina

Wei Shi
Department of Mechanical Engineering
Tsinghua University
Beijing, China

Caner Şimşir
Stiftung Institüt für Werkstofftechnik (IWT)
Bremen, Germany

Božo Smoljan
Department of Materials Science and Engineering
University of Rijeka
Rijeka, Croatia

Weimin Zhang
School of Materials Science and Engineering
Shanghai Jiao Tong University
Shanghai, China

1 Mathematical Fundamentals of Thermal Process Modeling of Steels

Jiansheng Pan and Jianfeng Gu

CONTENTS

Steels are usually under the action of multiple physical variable fields, such as temperature field, fluid field, electric field, magnetic field, plasm field, and so on during thermal processing. Thus, heat conduction, diffusion, phase transformation, evolution of microstructure, and mechanical deformation are simultaneously taken place inside. This chapter includes the mathematical fundamentals of the most widely used numerical analysis methods for the solution of partial differential equations (PDEs), and the basic knowledge of continuum mechanics, fluid mechanics, phase transformation kinetics, etc. All these are indispensable for the establishment of the coupled mathematical models and realization of numerical simulation of thermal processing.

1.1 THERMAL PROCESS PDEs AND THEIR SOLUTIONS

1.1.1 PDEs for Heat Conduction and Diffusion

The first step of computer simulation of thermal processing is to establish an accurate mathematical model, i.e., the PDEs and boundary conditions that can quantificationally describe the related phenomena.

The PDE describing the temperature field inside a solid is usually expressed as follows:

$$\frac{\partial}{\partial x}\left(\lambda\frac{\partial T}{\partial x}\right)+\frac{\partial}{\partial y}\left(\lambda\frac{\partial T}{\partial y}\right)+\frac{\partial}{\partial z}\left(\lambda\frac{\partial T}{\partial z}\right)+Q=\rho c_p\frac{\partial T}{\partial \tau} \tag{1.1}$$

where

T is the temperature
τ is the time
x, y, z are the coordinates
λ is the thermal conduction coefficient
ρ is the density
c_p is the heat capacity
Q is the intensity of the internal heat resource

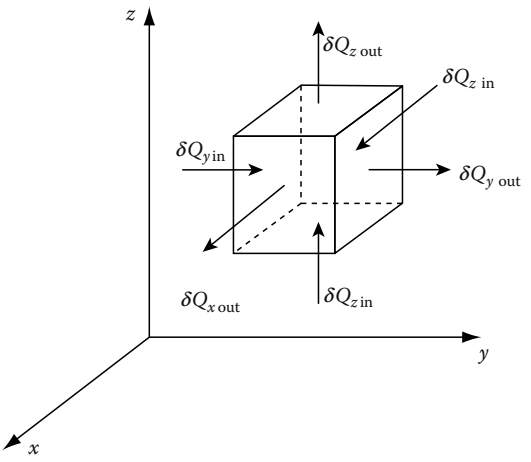

FIGURE 1.1 Heat flux along coordinates subjected to an infinitesimal element.

Equation 1.1 has a very clear physical concept, and can be illustrated as in Figure 1.1. The first item on the left-hand side of the equation is the net heat flux input to the infinitesimally small element along axis x, i.e., the difference between the heat flux entering $\delta Q_{x\text{in}}$ and the heat flux effusing $\delta Q_{x\text{out}}$. The second and third items are the net heat flux along axes y and z, respectively (Figure 1.1). The intensity of the internal heat source Q may be caused by different factors, such as phase transformation, plastic work, electricity current, etc. The right-hand side of the equation stands for the change in heat accumulating in the infinitesimal element per time unit due to the temperature change. Equation 1.1 shows that the sum of the heat input and heat generated by the internal heat source is equal to the change in heat accumulating for an infinitesimal element in each time unit, so it functions in accordance with the energy conservative law. The heat conduction coefficient λ, density ρ, heat capacity c_p, and the intensity of the internal heat source are usually the functions of temperature, making Equation 1.1 a nonlinear PDE.

There are three kinds of boundary conditions for heat exchange in all kinds of thermal processing technologies.

The first boundary condition S_1: The temperature of the boundary (usually certain surfaces) is known; it is a constant or function of time.

$$T_s = C(\tau) \tag{1.2}$$

The second boundary condition S_2: The heat flux of the boundary is known.

$$\lambda \frac{\partial T}{\partial n} = q \tag{1.3}$$

where

$\partial T/\partial n$ is the temperature gradient on the boundary along the external normal direction

q is the heat flux through the boundary surface

The third boundary condition S_3: The heat transfer coefficient between the workpiece and environment is known.

$$-\lambda\left(\frac{\partial T}{\partial n}\right) = h(T_a - T_s) \tag{1.4}$$

where

T_a is the environment temperature
T_s is the surface temperature of the workpiece
h is the overall heat transfer coefficient, representing the heat quantity exchanged between the workpiece surface and the environment per unit area and unit time when their temperature difference is 1°C

It is worth mentioning that only convective heat transfer occurs in some cases; however, radiation heat transfer should also be considered in other complicated ones, such as gas quenching and heating under protective atmosphere. Hence, the overall heat transfer coefficient h should be the sum of the convective heat transfer coefficient h_c and the radiation heat transfer coefficient h_r. Therefore, we have

$$h = h_c + h_r \tag{1.5}$$

The radiation heat transfer coefficient h_r can be obtained as follows:

$$h_r = \varepsilon\sigma(T_a^2 + T_s^2)(T_a + T_s) \tag{1.6}$$

where

ε is the radiation emissivity of the workpiece
σ is the Stefan–Boltzmann constant

The boundary condition can be set according to the specific thermal process, and the temperature field inside the workpiece at different times, the so-called unsteady temperature field, can be obtained by solving Equation 1.1. When the temperature field inside the workpiece does not change with time any more, it arrives at the steady temperature field, and the left-hand side of Equation 1.1 becomes zero.

The unsteady concentration field inside the workpiece subjected to carburizing or nitriding is usually governed by the following PDE.

$$\frac{\partial}{\partial x}\left(D\frac{\partial C}{\partial x}\right) + \frac{\partial}{\partial y}\left(D\frac{\partial C}{\partial y}\right) + \frac{\partial}{\partial z}\left(D\frac{\partial C}{\partial z}\right) = \frac{\partial C}{\partial \tau} \tag{1.7}$$

where

C is the concentration of the element being penetrated (carbon or nitrogen)
D is the diffusion coefficient

The boundary conditions can also be classified into the following three kinds.

Boundary s_1: The surface concentration is known.

$$C_s = C \tag{1.8}$$

Boundary s_2: The mass flux through the surface is known.

$$D\left(\frac{\partial C}{\partial n}\right) = q \tag{1.9}$$

Boundary s_3: The mass transfer coefficient between the workpiece surface and environment (ambient media) is known.

$$-D\left(\frac{\partial C}{\partial n}\right) = \beta(C_g - C_s) \tag{1.10}$$

where

D is the diffusion coefficient
β is the mass transfer coefficient
C_g is the atmosphere potential of carbon (or nitrogen)
C_s is the surface concentration of carbon (or nitrogen)

Although the diffusion and heat conduction PDEs describe different physical phenomena, their mathematical expression and solving method are exactly the same.

1.1.2 Solving Methods for PDEs

Usually, there are two methods to solve the PDEs, analytical method and numerical method. The analytical method, taking specific boundary conditions and initial conditions, can obtain the analytical solution by deduction (for example, variables separation method), which is a type of mathematical representation clearly describing certain field variables under space coordinates and time.

The analytical solution has the advantage of concision and accuracy, so it is also called exact solution. Although it plays an important role in fundamental research, it is only applicable to very few cases with relatively simple boundary and initial conditions. Therefore, the analytical solution cannot cope with massive problems under practical manufacture environment, which are featured with complicated boundary conditions and a high degree of nonlinearity.

The numerical solution, also named approximate solution, is applicable for different kinds of boundary conditions and can cope with nonlinear problems. It is the most basic simulation method in engineering. Up to now, the finite-element method (FEM) and finite-difference method (FDM) are the most widely used methods in simulation of the process, and their common characteristic is discretization of continuous functions, thus transforming the PDEs into large systems of simultaneous algebraic equations and solving the large algebraic equation group finally (Figure 1.2).

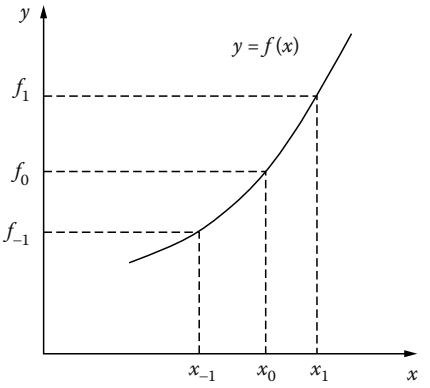

FIGURE 1.2 Discretization of the continuous function.

1.2 FINITE-DIFFERENCE METHOD

1.2.1 Introduction of FDM Principle

First, for a continuous function of x, namely $f(x)$, f_{-1}, f_0, and f_1 are retained as the values of f at x_{-1}, x_0, and x_1, respectively (Figure 1.2). When the function has all its derivatives defined at x_0 and f_1, f_{-1} can be expressed by a Taylor series as follows:

$$f_1 = f_0 + \Delta x \cdot f_0' + \frac{(\Delta x)^2}{2!} f_0'' + \frac{(\Delta x)^3}{3!} f_0''' + \frac{(\Delta x)^{i\mathrm{V}}}{4!} f_0^{i\mathrm{V}} + \cdots \tag{1.11}$$

$$f_{-1} = f_0 - \Delta x \cdot f_0' + \frac{(\Delta x)^2}{2!} f_0'' - \frac{(\Delta x)^3}{3!} f_0''' + \frac{(\Delta x)^{i\mathrm{V}}}{4!} f_0^{i\mathrm{V}} - \cdots \tag{1.12}$$

Truncating the items after $(\Delta x)^2$, Equation 1.11 can be written as

$$\left.\frac{\partial f}{\partial x}\right|_{x=x_0} = f_0' = \frac{f_1 - f_0}{\Delta x} - \frac{\Delta x}{2} f_0'' \approx \frac{f_1 - f_0}{\Delta x} \tag{1.13}$$

Equation 1.13 is the first-order forward difference with its truncation error of $\Omega(\Delta x)$. Here $\Omega(\Delta x)$ is a formal mathematical notation, which represents terms of order Δx.

In the same way, another difference scheme from Equation 1.12 can be obtained as follows:

$$\left.\frac{\partial f}{\partial x}\right|_{x=x_0} = f_0' = \frac{f_0 - f_{-1}}{\Delta x} + \frac{\Delta x}{2} f_0'' \approx \frac{f_0 - f_{-1}}{\Delta x} \tag{1.14}$$

This is the first-order backward difference with its truncation error of $\Omega(\Delta x)$.

Subtracting Equation 1.12 from Equation 1.11 yields

$$\frac{\partial f}{\partial x} = f_0' = \frac{f_1 - f_{-1}}{2} + 2\frac{(\Delta x)^2}{3!} f_0''' \approx \frac{f_1 - f_{-1}}{2} \tag{1.15}$$

Equation 1.15 is the second-order central difference with its truncation error of $\Omega(\Delta x^2)$.

Summing Equations 1.11 and 1.12, and solving for $\partial^2 f/\partial x^2$, we have

$$\frac{\partial^2 f}{\partial x^2} = f_0'' = \frac{f_1 - 2f_0 + f_{-1}}{(\Delta x)^2} + 2\frac{(\Delta x)^2}{4!} f_0^{i\mathrm{V}} \approx \frac{f_1 - 2f_0 + f_{-1}}{(\Delta x)^2} \tag{1.16}$$

Equation 1.16 is the second-order central second difference with its truncation error of $\Omega(\Delta x^2)$.

It can be observed that the truncation error, originating from the replacement of the partial derivatives by finite-difference quotients, makes the FDM solution an approximate one; however, the accuracy can be improved by reducing the step size.

1.2.2 FDM for One-Dimensional Heat Conduction and Diffusion

In this section, two simple cases are taken to elucidate the FDM to solve the PDEs in engineering. The first case is the unsteady, one-dimensional heat conduction PDE without an internal heat resource item, and the second one is the one-dimensional diffusion PDE.

The governing PDE for the unsteady, one-dimensional heat conduction without an internal heat resource item has the following concise form:

$$a\frac{\partial^2 T}{\partial x^2} = \frac{\partial T}{\partial \tau} \tag{1.17}$$

where $\alpha = \lambda / \rho c_p$, x and τ are independent variables. Equation 1.17 has two independent variables, x and τ.

Replacing the partial derivatives in Equation 1.17 with finite-difference quotients, the difference equation can be obtained as follows:

$$\frac{T_{i-1}^n - 2T_i^n + T_{i+1}^n}{(\Delta x)^2} = \frac{1}{a}\frac{T_i^{n+1} - T_i^n}{\Delta \tau} \tag{1.18}$$

where

i is the running index in the x direction
n is the running index in the τ direction

When one of the independent variables is a marching variable, such as τ in Equation 1.17, it is conventional to denote the running index for this marching variable by n and to display this index as a superscript in the finite-difference quotient (Figure 1.3), T_{i-1}^n, T_i^n, and T_{i+1}^n are the temperatures on node $i-1$, i, and $i+1$ at time level n, respectively, and T_i^{n+1} is the temperature on node $i+1$ at time level $n+1$.

With some rearrangement, this equation can be written as

$$T_i^{n+1} = F_0 T_{i+1}^n + F_0 T_{i-1}^n + (1 - 2F_0)T_i^n \tag{1.19}$$

where

$$F_0 = \frac{a\Delta t}{(\Delta x)^2} = \frac{\lambda \cdot \Delta t}{\rho c_p (\Delta x)^2}$$

Equation 1.19 is written with temperatures at time level n on the right-hand side and temperatures at time level $n+1$ on the left-hand side. Within the time-marching philosophy, all temperatures at level n are known and those at level $n+1$ are to be calculated. Of particular significance is that only one unknown T_i^{n+1} appears in Equation 1.19. Hence, Equation 1.19 allows for the immediate solution of T_i^{n+1} from the known temperatures at time level n.

Equation 1.19 is one of the so-called explicit finite-difference approaches, which provide a straightforward mechanism to accomplish this time marching (Figure 1.3). However, this approach

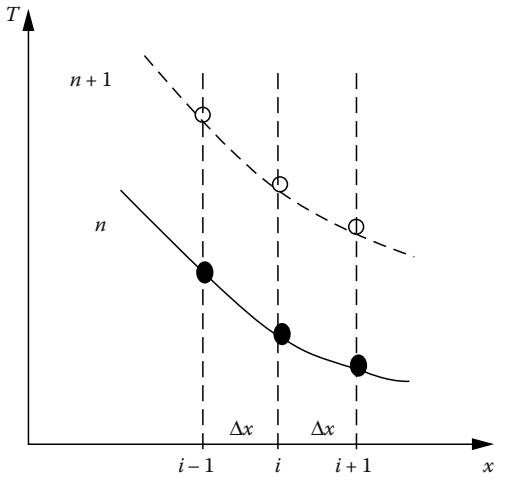

FIGURE 1.3 Illustration of discretization and time marching.

has the limitation that only when the stability criterion $F_0 \leq 1/2$ is met, the converged solution can be obtained. The truncation error can be estimated as $\Omega(\Delta x^2)(\Delta\tau)$.

Writing the spatial difference on the right-hand side of Equation 1.17 in terms of temperatures at time level $n+1$, we can obtain

$$a \cdot \frac{T_{i-1}^{n+1} - 2T_i^{n+1} + T_{i+1}^{n+1}}{(\Delta x)^2} = \frac{T_i^{n+1} - T_i^n}{\Delta\tau} \tag{1.20}$$

With some rearrangement, Equation 1.21 can be written as

$$F_0 T_{i-1}^{n+1} - (2F_0 + 1)T_i^{n+1} + F_0 T_{i-1}^{n+1} = T_i^n \tag{1.21}$$

Observing Equation 1.21, the unknown T_i^{n+1} is not only expressed in terms of the known temperatures at time level n, namely T_i^n, but also in terms of other unknown temperatures at time level $n+1$, namely, T_{i-1}^{n+1} and T_{i+1}^{n+1}. In other words, Equation 1.21 represents one equation with three unknowns, namely T_{i-1}^{n+1}, T_i^{n+1}, and T_{i+1}^{n+1}. Hence, Equation 1.21 applied at a given grid point i does not stand alone; it cannot by itself result in a solution for T_i^{n+1}. Rather, Equation 1.21 must be written at all interior grid points, resulting in a system of algebraic equations from which the unknowns T_i^{n+1} for all i can be solved simultaneously.

Equation 1.21 is one of the so-called implicit finite-difference approaches, in which the unknown must be obtained by means of simultaneous solution of the difference equations applied at all grid points arrayed at a given time level. Because of this need to solve large systems of simultaneous algebraic equations, implicit methods are usually involved with the manipulations of large matrices. One advantage of these methods lies in the fact that they are unconditionally stable, i.e., they can always get the converged solution. Their truncation error can also be estimated as $\Omega(\Delta x^2) \cdot (\Delta\tau)$.

There are different difference equations that can represent Equation 1.17 except Equations 1.21 and 1.22, which are the only two of many difference representations of the original PDE. For example, writing the spatial difference on the right-hand side in terms of average temperatures between time level n and $n+1$, Equation 1.17 can be represented by

$$\begin{aligned} &a\left[\frac{T_{i-1}^n - 2T_i^n + T_{i+1}^n}{2(\Delta x)^2} + \frac{T_{i-1}^{n+1} - 2T_i^{n+1} + T_{i+1}^{n+1}}{2(\Delta x)^2}\right] = \frac{T_i^{n+1} - T_i^n}{\Delta t} \\ &\quad - F_0 T_{i-1}^{n+1} + 2(1+F_0)T_i^{n+1} - F_0 T_{i+1}^{n+1} = F_0 T_{i-1}^n + 2(1-F_0)T_i^n + F_0 T_{i+1}^n \end{aligned} \tag{1.22}$$

This special type of differencing employed in Equation 1.22 is called the Crank–Nicolson form, which is also unconditionally stable and has a small truncation error of $\Omega(\Delta x)^2(\Delta\tau)^2$.

As a typical case of one-dimensional heat conduction without an internal heat resource, an infinite plate with a thickness of δ is subjected to the boundary condition that can be expressed as follows:

$$h(T_a - T_s) = -\lambda \left.\frac{\partial T}{\partial n}\right|_{x=0} \tag{1.23}$$

The spatial discretization is shown in Figure 1.4, generating $m+1$ nodes from surface (node 0) to center (node m). Here, because of the symmetry half of the slab can only be considered, and the symmetry axis can be set as the adiabatical boundary.

For the surface node ($i=0$), the boundary condition is introduced and the Crank–Nicolson form can be obtained as follows:

$$h\left[T_a - \frac{1}{2}\left(T_0^{n+1} + T_0^n\right)\right] - \frac{\lambda}{2\Delta x}\left(T_0^{n+1} - T_1^{n+1} + T_0^n - T_1^n\right) = \frac{\Delta x \rho c_p}{2\Delta t}\left(T_0^{n+1} - T_0^n\right) \tag{1.24}$$

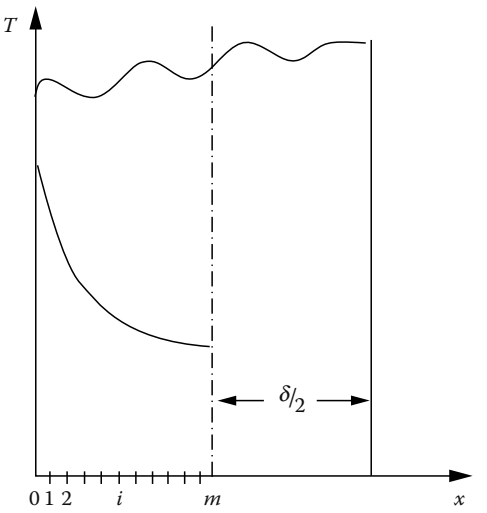

FIGURE 1.4 Spatial difference scheme of nodes for an infinite plate.

With some rearrangement, Equation 1.24 can be written as

$$(1 + F_0 + Bi)T_0^{n+1} - F_0T_1^{n+1} = (1 - F_0 - Bi)T_0^n + F_0T_1^n + 2BiT_a \tag{1.25}$$

where $Bi = h\Delta t/\Delta x$.

For the central node ($i = m$), the adiabatical boundary $\partial T/\partial x = 0$ is input, and the difference equation is

$$(1 + F_0)T_{m-1}^{n+1} - F_0T_{m-1}^{n+1} = (1 - F_0)T_m^n + F_0T_{m-1}^n \tag{1.26}$$

The finite-difference form for transient heat conduction in the infinite plate is composed by Equations 1.22, 1.25, and 1.26, providing $m + 1$ algebraic equations for $m + 1$ unknown T_i for all nodes. The unique solution for the temperature field can usually be obtained by a mature algorithm.

The one-dimensional diffusion PDE (Equation 1.27) and its difference equations have the same form as that of the unsteady, one-dimensional heat conduction without an internal heat resource. Hence, the corresponding equations are briefly repeated and then entered into solving of the algebraic equation group.

$$D\frac{\partial^2 C}{\partial X^2} = \frac{\partial C}{\partial \tau} \tag{1.27}$$

The boundary conditions at the surface node and the center node are the third type of boundary condition and the adiabatical condition, respectively, and are listed as follows:

$$\begin{cases} -D\left.\dfrac{\partial C}{\partial X}\right|_{x=0} = \beta(C_g - C_s) \\ D\left.\dfrac{\partial C}{\partial X}\right|_{x=m} = 0 \end{cases} \tag{1.28}$$

For the inner nodes ($i = 1 \cdots m-1$), the Crank–Nicolson difference form can be written as

$$-F_0 C_{i-1}^{n+1} + 2(1+F_0)C_i^{n+1} - F_0 C_{i+1}^{n+1} = F_0 C_{i-1}^{n} + 2(1-F_0)C_i^{n} + F_0 C_{i+1}^{n} \tag{1.29}$$

where $F_0 = \dfrac{(D \cdot \Delta\tau)}{(\Delta x)^2}$.

For the surface node ($i = 0$), the Crank–Nicolson form is

$$(1 + F_0 + Bi)C_0^{n+1} - F_0 C_1^{n+1} = (1 - F_0 - Bi)C_0^{n} + F_0 C_1^{n} + 2BiC_g \tag{1.30}$$

For the central node ($i = m$), the difference equation is

$$(1+F_0)C_m^{n+1} - F_0 C_{m-1}^{n+1} = (1-F_0)C_m^{n} + F_0 C_{m-1}^{n} \tag{1.31}$$

The algebraic equation group constituted by Equations 1.29 through 1.31 can be expanded and written in the following matrix form:

$$\begin{bmatrix} d_0 & a_0 & & & & & & \\ b_1 & d_1 & a_1 & & & & & \\ & \ddots & \ddots & \ddots & & & & \\ & & b_i & d_i & a_i & & & \\ & & & \ddots & \ddots & \ddots & & \\ & & & & b_{m-1} & d_{m-1} & a_{m-1} & \\ & & & & & b_m & d_m & \end{bmatrix} \begin{bmatrix} C_0 \\ C_1 \\ \vdots \\ C_i \\ \vdots \\ C_{m-1} \\ C_m \end{bmatrix}$$

$$= \begin{bmatrix} d'_0 & a'_0 & & & & & & \\ b'_1 & d'_1 & a'_1 & & & & & \\ & \ddots & \ddots & \ddots & & & & \\ & & b'_i & d'_i & a'_i & & & \\ & & & \ddots & \ddots & \ddots & & \\ & & & & b'_{m-1} & d'_{m-1} & a'_{m-1} & \\ & & & & & b'_m & d'_m & \end{bmatrix} \times \begin{bmatrix} C_0 \\ C_1 \\ \vdots \\ C_i \\ \vdots \\ C_{m-1} \\ C_m \end{bmatrix}^n + \begin{bmatrix} 2lC_0 \\ 0 \\ \vdots \\ 0 \\ \vdots \\ 0 \\ 0 \end{bmatrix} \tag{1.32}$$

where

$$d_0 = 1 + F_0 + Bi$$
$$d_1 = d_2 = \cdots = d_{m-1} = 2(1+F_0)$$
$$d_m = 1 + F_0$$
$$b_1 = b_2 = \cdots = b_m = -F_0$$
$$a_0 = a_1 = \cdots = a_{m-1} = -F_0$$
$$d'_0 = 1 - F_0 - Bi$$
$$d'_1 = d'_2 = \cdots = d'_{m-1} = 2(1-F_0)$$
$$d'_m = 1 - F_0$$
$$b'_1 = b'_2 = \cdots = b'_m = F_0$$
$$a'_0 = a'_1 = \cdots = a'_{m-1} = -F$$

When the concentration of the nodes at time level n is known, the right-hand side of Equation 1.32 can be simplified as a column matrix. Thus, we obtain

$$\begin{bmatrix} d_0 & a_0 & & & & & & \\ b_1 & d_1 & a_1 & & & & & \\ & \ddots & \ddots & \ddots & & & & \\ & & b_i & d_i & a_i & & & \\ & & & \ddots & \ddots & \ddots & & \\ & & & & b_{m-1} & d_{m-1} & a_{m-1} & \\ & & & & & b_m & d_m & \end{bmatrix} \begin{bmatrix} C_0 \\ C_1 \\ \vdots \\ C_i \\ \vdots \\ C_{m-1} \\ C_m \end{bmatrix}^{n+1} = \begin{bmatrix} F_0 \\ F_1 \\ \vdots \\ F_i \\ \vdots \\ F_{m-1} \\ F_m \end{bmatrix} \tag{1.33}$$

The coefficient matrix on the left-hand side of Equation 1.33 is a tridiagonal matrix, defined as having nonzero elements only along the three diagonals, which are marked with three dashed lines. The solution of the system of equations denoted by Equation 1.33 involves the manipulation of the tridiagonal arrangement; such solutions are usually obtained using Thomas' algorithm, which has become almost standard for the treatment of tridiagonal systems of equations. A description of this algorithm is given as follows.

First, Equation 1.33 is changed into an upper bidiagonal form by dropping the first term of each equation, replacing the coefficient of the main-diagonal term by Equation 1.34, and replacing the right-hand side with Equation 1.35.

$$d_i^* = d_i - \frac{b_i}{d_{i-1}^*} a_{i-1} \quad (i = 1, 2, 3, \ldots, m-1, m) \tag{1.34}$$

$$F_i^* = F_i - \frac{b_i}{d_{i-1}^*} F_{i-1}^* \quad (i = 1, 2, 3, \ldots, m-1, m) \tag{1.35}$$

Then Equation 1.33 transforms into an upper bidiagonal form as follows:

$$\begin{bmatrix} d_0 & a_0 & & & & \\ & d_1^* & a_1 & & & \\ \ddots & \ddots & \ddots & & & \\ & & d_i^* & a_i & & \\ & \ddots & \ddots & \ddots & & \\ & & & d_{m-1}^* & a_{m-1} & \\ & & & & d_m^* & \end{bmatrix} \begin{bmatrix} C_0 \\ C_1 \\ \vdots \\ C_i \\ \vdots \\ C_{m-1} \\ C_m \end{bmatrix}^{n+1} = \begin{bmatrix} F_0 \\ F_1^* \\ \vdots \\ F_i^* \\ \vdots \\ F_{m-1}^* \\ F_m^* \end{bmatrix} \tag{1.36}$$

The elements with the superscript asterisk are those subjected to Gaussian elimination. The last equation in Equation 1.36 has only one unknown. Solving C_m^{n+1} from Equation 1.37, all other unknowns are found in sequence from Equation 1.38, starting from C_{m-1}^{n+1} to C_1^{n+1}.

$$C_m^{n+1} = \frac{F_m^*}{d_m^*} \tag{1.37}$$

$$C_i^{n+1} = \frac{\left(F_i^* - a_i C_{i+1}^{n+1}\right)}{d_i^*} \quad (i = m-1, m-2, \ldots, 2, 1) \tag{1.38}$$

The concentration of the surface node C_0^{n+1} can be obtained by

$$C_0^{n+1} = \frac{\left(F_0 - a_0 C_1^{n+1}\right)}{d_0} \tag{1.39}$$

So far, the concentration of all nodes at time level $n+1$ has been calculated. Sometimes, the activity is used instead of the concentration in diffusion problems such as the nitriding process.

1.2.3 Brief Summary

The main advantage of FDM lies in its rigorous mathematical derivation, and it is very simple when applied in one-dimensional problems. For the two- and three-dimensional problems, FDM can also be applied but for objects with relatively simple shapes due to its limitation in coping with complicated-shape boundaries. Hence, the FEM method is mainly used in the simulation of temperature fields and concentration fields with three-dimensional complicated-shape parts.

1.3 FINITE-ELEMENT METHOD

The FEM, sometimes referred to as finite-element analysis (FEA), is a computational technique used to obtain approximate solutions of boundary value problems in engineering. Simply stated, a boundary value problem is a mathematical problem in which one or more dependent variables must satisfy a differential equation everywhere within a known domain of independent variables and satisfy specific conditions on the boundary of the domain. Usually, FEM divides the definition domain into reasonably defined subdomains (element) by hypothesis and supposes the unknown state variable function in each element approximately defined, so that the approximate solution of boundary value and initial value problems is thus obtained. Since the respectively defined functions can be harmonized at element nodes or certain joint points, the unknown function can approximately be expressed in the whole definition domain.

Because of the extraordinary flexibility of element division, the FEM elements can fit well to objects with complex shape and the boundaries with complex curved surfaces. For example, complex three-dimensional regions can be effectively filled by tetrahedral elements, similar to triangular elements filling a two-dimensional region. Therefore, the FEM is the most widely used method in heat treatment numerical simulation so far.

FEM has been dissertated in detail in related monographs [1–3]. Hence, a brief introduction is presented in this section.

1.3.1 Brief Introduction

No matter what the physical nature of the problem, the standard FEM is always performed with a sequential series of steps. Certain steps in formulating an FEA of a physical problem are common to all such analyses, whether structural, heat transfer, fluid flow, or some other problems. The steps are described as follows:

1. Definition of problem and its definition domain
2. Discretization of the definition domain
3. Determination of all kinds of state variables
4. Formulations of the problem
5. Establishing of coordinate system
6. Construction of the approximate function for elements
7. Derivation of element matrix and equation

8. Coordinate transformation
9. Assembly of element equation
10. Introduction of the boundary condition
11. Solution to the final algebraic equation
12. Explanation of the results

When FEM for a specific engineering problem is performed by computer (these steps are embodied in commercial finite-element software packages), it usually involves three stages of activity: preprocessing, solution, and postprocessing.

1.3.1.1 Stage 1: Preprocessing

The preprocessing stage involves the preparation of data, such as nodal coordinates, connectivity, boundary conditions, loading, and materials information. It is generally described as defining the model and includes the following:

- Define the geometric domain of the problem
- Define the element type(s) to be used
- Define the material properties of the elements
- Define the geometric properties of the elements (length, area, and the like)
- Define the element connectivities (mesh of the model)
- Define the physical constraints (boundary conditions)
- Define the loadings

1.3.1.2 Stage 2: Solution

The solution stage involves stiffness generation, stiffness modification, and solution of equations, resulting in the evaluation of nodal variables. Other derived quantities, such as gradients for stresses, may be evaluated at this stage. In other words, the finite-element software assembles the governing algebraic equations in matrix form and computes the unknown values of the primary field variable(s). The computed values are then used by back substitution to compute additional derived variables, such as reaction forces, element stresses, and heat flow.

1.3.1.3 Stage 3: Postprocessing

Analysis and evaluation of the solution results is referred to as postprocessing, so the postprocessing stage deals with the presentation of results. Typically, the deformed configuration, mode shapes, temperature, and stress distribution are computed and displayed at this stage. Postprocessor software contains sophisticated routines used for sorting, printing, and plotting selected results from a finite-element solution. Examples of operations that can be accomplished include

- Sort element stresses in order of magnitude
- Check equilibrium
- Calculate factors of safety
- Plot deformed structural shape
- Animate dynamic model behavior
- Produce color-coded temperature plots

While solution data can be manipulated in many ways in postprocessing, the most important objective is to apply sound engineering judgment in determining whether the solution results are physically reasonable.

1.3.2 Galerkin FEM for Two-Dimensional Unsteady Heat Conduction

The method of weighted residuals, especially the embodiment of the Galerkin FEM, is a powerful mathematical tool that provides a technique for formulating a finite-element solution approach to practically any problem for which the governing differential equation and boundary conditions can be written.

Here, two-dimensional unsteady heat conduction is taken as an example to derive the FEM formulations by Galerkin's weighted residual method.

The governing PDE for unsteady, two-dimensional heat conduction with an internal heat resource is

$$\lambda\left(\frac{\partial^2 T}{\partial x^2}+\frac{\partial^2 T}{\partial y^2}\right)+Q-\rho c_p\frac{\partial T}{\partial \tau}=0 \tag{1.40}$$

The initial condition, supposing the temperature field is known, can be written as

$$\tau=0:\quad T=T_0 \tag{1.41}$$

The three types of boundary conditions have been listed by Equations 1.2 through 1.4.

The right-hand side of Equation 1.40 equals zero when the column vector T, the exact solution of the temperature field, is substituted. On the contrary, the approximate solution T makes the residual error:

$$R=\lambda\left(\frac{\partial^2 T}{\partial x^2}+\frac{\partial^2 T}{\partial y^2}\right)+Q-\rho c_p\frac{\partial T}{\partial \tau} \tag{1.42}$$

The basic idea of the weighted residual method is to construct a suitable weight function so that the integration of products by residual error and weight function equals zero; the approximate solution on the whole domain can thus be obtained. Therefore, we have

$$\iint_D W_i\left(\lambda\left(\frac{\partial^2 T}{\partial x^2}+\frac{\partial^2 T}{\partial y^2}\right)-\rho c_p\frac{\partial T}{\partial \tau}+Q\right)\mathrm{d}x\,\mathrm{d}y=0 \tag{1.43}$$

where W_i is the weight function.

Several variations of the weighted residual method exist and the techniques vary primarily in how the weight functions are determined or selected. The most common techniques are point collocation, subdomain collocation, least squares, and Galerkin's method [4].

The second-order differential item in Equation 1.43 can be transformed into a first-order item by integration in parts. Therefore, the second-order differential item can be expressed as

$$\iint_D W_i\left(\lambda\left(\frac{\partial^2 T}{\partial x^2}+\frac{\partial^2 T}{\partial y^2}\right)\right)\mathrm{d}x\,\mathrm{d}y=-\iint_D\lambda\left(\frac{\partial W_i}{\partial x}\frac{\partial T}{\partial x}+\frac{\partial W_i}{\partial y}\frac{\partial T}{\partial y}\right)\mathrm{d}x\,\mathrm{d}y+\int_S W_i\lambda\frac{\partial T}{\partial n}\mathrm{d}s \tag{1.44}$$

and

$$\int_S W_i\lambda\frac{\partial T}{\partial n}\mathrm{d}s=\int_{S_1} W_i\lambda\frac{\partial T}{\partial n}\mathrm{d}s+\int_{S_2} W_i\lambda\frac{\partial T}{\partial n}\mathrm{d}s+\int_{S_3} W_i\lambda\frac{\partial T}{\partial n}\mathrm{d}s \tag{1.45}$$

Since the temperature on boundary S_1 is known, we have $\int_{S_1} W_i\lambda(\partial T/\partial n)\mathrm{d}s = 0$. Substituting Equations 1.44 and 1.45 into Equation 1.43, we can get

$$\iint_D \lambda\left(\frac{\partial W_i}{\partial x}\frac{\partial T}{\partial x}+\frac{\partial W_i}{\partial y}\frac{\partial T}{\partial y}\right)\mathrm{d}x\,\mathrm{d}y + W_i\left(\rho c_p\frac{\partial T}{\partial \tau}-Q\right)\mathrm{d}x\,\mathrm{d}y = \int_{S_2} W_i\lambda\frac{\partial T}{\partial n}\mathrm{d}s + \int_{S_3} W_i\lambda\frac{\partial T}{\partial n}\mathrm{d}s \quad (1.46)$$

The element analysis is to establish the formulations by which the continuous function in the subdomain ΔD can be expressed by the node values, i.e., the function of the node values. Supposing there are n elements in the solution domain, and there are m nodes in each element with the temperature T_i ($i = 1, 2, \ldots, m$), the unknown temperature $T^{\mathrm{e}}_{(x,y,z)}$ defined in the element can be expressed as the interpolation function of each node. Therefore, we have

$$T^{\mathrm{e}}_{(x,y,z)} = N_1T_1 + N_2T_2 + \cdots + N_mT_m = [N_i]\{T_i\} \quad (1.47)$$

where N_i is the shape function, which is a function of the components of each element nodes (x_i, y_i, z_i) and those of the location (x, y, z).

For example, the shape functions of a triangle element with three nodes can be simply derived and expressed as

$$\begin{aligned} N_i(x,y) &= \frac{1}{2A}(a_i + b_ix + c_iy)\\ N_j(x,y) &= \frac{1}{2A}(a_j + b_jx + c_jy)\\ N_m(x,y) &= \frac{1}{2A}(a_m + b_mx + c_my) \end{aligned} \quad (1.48)$$

where

$A = \frac{1}{2}(b_ic_j - b_jc_i)$
$a_i = x_jy_m - x_my_j$; $a_j = x_my_i - x_iy_m$; $a_m = x_iy_j - x_jy_i$
$b_i = y_j - y_m$; $b_j = y_m - y_i$; $b_m = y_i - y_j$
$c_i = x_m - x_j$; $c_j = x_i - x_m$; $c_m = x_j - x_i$

Although the shape functions for different types of elements have different forms, they have common characteristics and can be obtained by the geometrical method. Especially the coefficients in the shape functions are the functions of the coordinates of each node, that is,

$$N_i(x,y,z) = F(x_i,y_i,z_i,x,y,z), \quad i = 1,2,\ldots,m \quad (1.49)$$

Obviously, the shape functions are determined only by the coordinates of each node and the type of element. Hence, the temperature on certain points in an element can be expressed as the function of node temperature, namely, the column vector $\{T_i\}$ (see Equation 1.47).

Equation 1.46 is applicable in the whole solution domain D, so for its subdomains, i.e., each element ΔD, we have

$$\begin{aligned} &\iint_{\Delta D} \lambda\left(\frac{\partial W_i}{\partial x}\frac{\partial T}{\partial x}+\frac{\partial W_i}{\partial y}\frac{\partial T}{\partial y}\right)\mathrm{d}x\,\mathrm{d}y + W_i\left(\rho c_p\frac{\partial T}{\partial \tau}-Q\right)\mathrm{d}x\,\mathrm{d}y\\ &\quad = \int_{\Delta S_2} W_i\lambda\frac{\partial T}{\partial n}\mathrm{d}s + \int_{\Delta S_3} W_i\lambda\frac{\partial T}{\partial n}\mathrm{d}s \end{aligned} \quad (1.50)$$

In Galerkin's weighted residual method, the weight functions are chosen to be identical to the trial function. Here, the shape functions are taken as the weight functions, for example, $W_i = N_i(x, y)$, and substitute into Equation 1.50. Hence, we have

$$\iint_{\Delta D} \lambda \left(\frac{\partial N_i}{\partial x} \frac{\partial T}{\partial x} + \frac{\partial N_i}{\partial y} \frac{\partial T}{\partial y} \right) \mathrm{d}x\,\mathrm{d}y + N_i \left(\rho c_p \frac{\partial T}{\partial \tau} - Q \right) \mathrm{d}x\,\mathrm{d}y = \int_{\Delta S_2} N_i \lambda \frac{\partial T}{\partial n} \mathrm{d}s + \int_{\Delta S_3} N_i \lambda \frac{\partial T}{\partial n} \mathrm{d}s \tag{1.51}$$

Substituting Equation 1.47 into Equation 1.51, and introducing the boundary conditions from Equations 1.2 through 1.4, we have

$$\begin{aligned} &\iint_{\Delta D} \left[\lambda \frac{\partial N_i}{\partial x} \left(\frac{\partial N_i}{\partial x} T_i + \frac{\partial N_j}{\partial x} T_j + \frac{\partial N_m}{\partial x} T_m \right) + \lambda \frac{\partial N_i}{\partial y} \left(\frac{\partial N_i}{\partial y} T_i + \frac{\partial N_j}{\partial y} T_j + \frac{\partial N_m}{\partial y} T_m \right) \right. \\ &\quad \left. + N_i \rho c_p \cdot \left(N_i \frac{\partial T_i}{\partial \tau} + N_j \frac{\partial T_j}{\partial \tau} + N_m \frac{\partial T_m}{\partial \tau} \right) - N_i Q \right] \mathrm{d}x\,\mathrm{d}y \\ &= \int_{\Delta S_2} q N_i \mathrm{d}s - \int_{\Delta S_3} h N_i (N_i T_i + N_j T_j - Ta) \mathrm{d}s \end{aligned} \tag{1.52}$$

Taking $W_j = N_j(x, y)$ and $W_m = N_m(x, y)$, and deriving in exactly the same way, can be obtained as follows:

$$\begin{aligned} &\iint_{\Delta D} \left[\lambda \frac{\partial N_j}{\partial x} \left(\frac{\partial N_i}{\partial x} T_i + \frac{\partial N_j}{\partial x} T_j + \frac{\partial N_m}{\partial x} T_m + \lambda \frac{\partial N_j}{\partial y} \right) \left(\frac{\partial N_i}{\partial y} T_i + \frac{\partial N_j}{\partial y} T_j + \frac{\partial N_m}{\partial y} T_m \right) \right. \\ &\quad \left. + N_j \rho c_p \left(N_i \frac{\partial T_i}{\partial \tau} + N_j \frac{\partial T_j}{\partial \tau} + N_m \frac{\partial T_m}{\partial \tau} \right) - N_i Q \right] \mathrm{d}x\,\mathrm{d}y \\ &= \int_{\Delta S_2} q N_j \mathrm{d}s - \int_{\Delta S_3} h N_j (N_i T_i + N_j T_j - Ta) \mathrm{d}s \end{aligned} \tag{1.53}$$

$$\begin{aligned} &\iint_{\Delta D} \left[\lambda \frac{\partial N_m}{\partial x} \left(\frac{\partial N_i}{\partial x} T_i + \frac{\partial N_j}{\partial x} T_j + \frac{\partial N_m}{\partial x} T_m \right) + \lambda \frac{\partial N_m}{\partial y} \left(\frac{\partial N_i}{\partial y} T_i + \frac{\partial N_j}{\partial y} T_j + \frac{\partial N_m}{\partial y} T_m \right) \right. \\ &\quad \left. + N_m \rho c_p \left(N_i \frac{\partial T_i}{\partial \tau} + N_j \frac{\partial T_j}{\partial \tau} + N_m \frac{\partial T_m}{\partial \tau} \right) - N_i Q \,\mathrm{d}x\,\mathrm{d}y \right] \\ &= \int_{\Delta S_2} q N_m \mathrm{d}s - \int_{\Delta S_3} h N_m (N_i T_i + N_j T_j - Ta) \mathrm{d}s \end{aligned} \tag{1.54}$$

For the interior elements, the right-hand side of Equations 1.52 through 1.54 equals zero respectively; while for the boundary element, only the right-hand side of Equation 1.54 equals zero with the assumption that only node i and j are on the boundary.

An equation group constructed by Equations 1.52 through 1.54 contains only the three unknowns, T_i, T_j, and T_m. After rearrangement, it can be written in matrix form as follows:

$$[K]^{\mathrm{e}} \{T^{\mathrm{e}}\} + [C]^{\mathrm{e}} \frac{\partial}{\partial \tau} \{T\}^{\mathrm{e}} = \{\rho\}^{\mathrm{e}} \tag{1.55}$$

where

$[K]^e$ is the element stiffness matrix

$\{T\}^e$ is the column vector of temperature on element nodes (unknown)

$[C]^e$ is the element heat capacity matrix

$\{\rho\}^e$ is the element constant vector item

The element stiffness matrix assembled from Equations 1.52 through 1.54 is

$$[K]^e = \iint_{\Delta D} \lambda \begin{bmatrix} \frac{\partial N_i}{\partial x}\cdot\frac{\partial N_i}{\partial x}+\frac{\partial N_i}{\partial y}\cdot\frac{\partial N_i}{\partial y} & \frac{\partial N_j}{\partial x}\cdot\frac{\partial N_i}{\partial x}+\frac{\partial N_j}{\partial y}\cdot\frac{\partial N_i}{\partial y} & \frac{\partial N_m}{\partial x}\cdot\frac{\partial N_i}{\partial x}+\frac{\partial N_m}{\partial y}\cdot\frac{\partial N_i}{\partial y} \\ \frac{\partial N_i}{\partial x}\cdot\frac{\partial N_j}{\partial x}+\frac{\partial N_i}{\partial y}\cdot\frac{\partial N_j}{\partial y} & \frac{\partial N_j}{\partial x}\cdot\frac{\partial N_j}{\partial x}+\frac{\partial N_j}{\partial y}\cdot\frac{\partial N_j}{\partial y} & \frac{\partial N_m}{\partial x}\cdot\frac{\partial N_j}{\partial x}+\frac{\partial N_m}{\partial y}\cdot\frac{\partial N_j}{\partial y} \\ \frac{\partial N_i}{\partial x}\cdot\frac{\partial N_m}{\partial x}+\frac{\partial N_i}{\partial y}\cdot\frac{\partial N_m}{\partial y} & \frac{\partial N_j}{\partial x}\cdot\frac{\partial N_m}{\partial x}+\frac{\partial N_j}{\partial y}\cdot\frac{\partial N_m}{\partial y} & \frac{\partial N_m}{\partial x}\cdot\frac{\partial N_m}{\partial x}+\frac{\partial N_m}{\partial y}\cdot\frac{\partial N_m}{\partial y} \end{bmatrix} \mathrm{d}x\,\mathrm{d}y + \int_{\Delta S_2} q \begin{bmatrix} N_i \\ N_j \\ 0 \end{bmatrix} \mathrm{d}s + \int_{\Delta S_3} h \begin{bmatrix} N_iN_i & N_jN_i & 0 \\ N_iN_j & N_jN_j & 0 \\ 0 & 0 & 0 \end{bmatrix} \mathrm{d}s \tag{1.56}$$

Substituting Equation 1.48 into Equation 1.56, and integrating, we obtain

$$[K]^e = \frac{\lambda}{4A}\begin{bmatrix} b_i^2+c_i^2 & b_ib_j+c_ic_j & b_ib_m+c_ic_m \\ b_jb_i+c_jc_i & b_j^2+c_j^2 & b_jb_m+c_jc_m \\ b_mb_i+c_mc_i & b_mb_j+c_mc_j & b_m^2+c_m^2 \end{bmatrix} + \frac{hl_{ij}}{6}\begin{bmatrix} 2 & 1 & 0 \\ 1 & 2 & 0 \\ 0 & 0 & 0 \end{bmatrix} \tag{1.57}$$

where

A is the area of element ΔD

l_{ij} is the length of exterior boundary; $l_{ij}=0$ for the interior element

The coefficients b_i, b_j, b_m, c_i, c_j, c_m are determined by the coordinates of nodes. Obviously, every element in $[K]^e$ is determined.

For the element heat capacity matrix, we have

$$[C]^e = \iint_{\Delta D} \rho C_p \begin{bmatrix} N_iN_i & N_jN_i & N_mN_i \\ N_iN_j & N_jN_j & N_mN_j \\ N_iN_m & N_jN_m & N_mN_m \end{bmatrix} \mathrm{d}x\,\mathrm{d}y \tag{1.58}$$

Substituting Equation 1.48 into Equation 1.58, and integrating, we obtain

$$\begin{aligned} \iint_{\Delta D} N_iN_j\,\mathrm{d}x\,\mathrm{d}y &= \iint_{\Delta D} N_iN_m\,\mathrm{d}x\,\mathrm{d}y = \iint_{\Delta D} N_jN_m\,\mathrm{d}x\,\mathrm{d}y = \frac{A}{12} \\ \iint_{\Delta D} N_iN_i\,\mathrm{d}x\,\mathrm{d}y &= \iint_{\Delta D} N_jN_j\,\mathrm{d}x\,\mathrm{d}y = \iint_{\Delta D} N_mN_m\,\mathrm{d}x\,\mathrm{d}y = \frac{A}{6} \end{aligned} \tag{1.59}$$

Thus, Equation 1.58 can be rewritten as

$$[C]^e = \frac{\rho c_p A}{12}\begin{bmatrix} 2 & 1 & 1 \\ 1 & 2 & 1 \\ 1 & 1 & 2 \end{bmatrix} \tag{1.60}$$

The element constant vector item $\{\rho\}^{\mathrm{e}}$ in Equation 1.55 can be expanded as

$$\{p\}^{\mathrm{e}} = \{p_{\mathrm{Q}}\}^{\mathrm{e}} + \{p_{\mathrm{q}}\}^{\mathrm{e}} + \{p_{\mathrm{h}}\}^{\mathrm{e}} \tag{1.61}$$

where $\{p_{\mathrm{Q}}\}^{\mathrm{e}}$, $\{p_{\mathrm{q}}\}^{\mathrm{e}}$, $\{p_{\mathrm{h}}\}^{\mathrm{e}}$ originate from the internal heat resource, heat flux in the second kind of boundary condition, and the heat transfer coefficient in the third kind of boundary condition, respectively.

The item $\{p_{\mathrm{Q}}\}^{\mathrm{e}}$ can be obtained by

$$\{p_{\mathrm{Q}}\}^{\mathrm{e}} = \int_{\Delta D} QN_i \,\mathrm{d}x\,\mathrm{d}y + \int_{\Delta D} QN_j \,\mathrm{d}x\,\mathrm{d}y + \int_{\Delta D} QN_m \,\mathrm{d}x\,\mathrm{d}y \tag{1.62}$$

When the internal heat resource intensity Q is a constant, we have

$$\{P_{\mathrm{Q}}\}^{\mathrm{e}} = \frac{AQ}{3}\begin{Bmatrix} 1 \\ 1 \\ 1 \end{Bmatrix} \tag{1.63}$$

When the internal heat resource intensity Q is a linear function, we have

$$\{P_{\mathrm{Q}}\}^{\mathrm{e}} = \frac{A}{12}\begin{bmatrix} 2Q_i & Q_j & Q_m \\ Q_i & 2q_j & Q_m \\ Q_i & Q_j & 2Q_m \end{bmatrix} \tag{1.64}$$

where Q_i, Q_j, and Q_m are the internal heat resource intensity on node i, j, and m, respectively.

The item $\{p_{\mathrm{q}}\}^{\mathrm{e}}$ due to the heat flux on the boundary can be obtained by

$$\{p_{\mathrm{q}}\}^{\mathrm{e}} = \int_{\Delta S_2} qN_i \,\mathrm{d}s + \int_{\Delta S_2} qN_j \,\mathrm{d}s + \int_{\Delta S_2} qN_m \,\mathrm{d}s \tag{1.65}$$

When the heat flux through the boundary q is a constant, we have

$$\{p_{\mathrm{q}}\}^{\mathrm{e}} = \frac{l_{ij}}{2}q\begin{Bmatrix} 1 \\ 1 \\ 0 \end{Bmatrix} \tag{1.66}$$

When the heat flux through the boundary q is a linear function, we have

$$\{p_{\mathrm{q}}\}^{\mathrm{e}} = \frac{l_{ij}}{6}q\begin{Bmatrix} 2q_i + q_j \\ q_i + 2q_j \\ 0 + 0 \end{Bmatrix} \tag{1.67}$$

The item $\{p_{\mathrm{h}}\}^{\mathrm{e}}$ due to the heat transfer coefficient on the boundary can be obtained by

$$\{p_{\mathrm{h}}\}^{\mathrm{e}} = \int_{\Delta C_3} hT_{\mathrm{a}}N_i \,\mathrm{d}s + \int_{\Delta C_3} hT_{\mathrm{a}}N_j \,\mathrm{d}s + \int_{\Delta C_3} hT_{\mathrm{a}}N_m \,\mathrm{d}s = \frac{l_{ij}}{2}hT_{\mathrm{a}}\begin{Bmatrix} 1 \\ 1 \\ 0 \end{Bmatrix} \tag{1.68}$$

Therefore, the continuous function $T^{e}_{(x,y,\tau)}$ on the subdomains, i.e., the element ΔD, has been expressed by the node temperature, and the algebraic equation group with the unknown variables of node temperature has been established.

For the whole solution domain, the algebraic equation groups on each element are assembled together so that a large-scale equation group can be obtained as follows:

$$[K]\{T\} + [C]\frac{\partial}{\partial \tau}\{T\} - \{P\} = 0 \tag{1.69}$$

where

$$\text{General stiffness matrix: } [K] = \sum [K]^{e} \tag{1.69a}$$

$$\text{Heat capacity matrix: } [C] = \sum [C]^{e} \tag{1.69b}$$

$$\text{Heat flux matrix: } \{P\} = \sum \{P\}^{e} \tag{1.69c}$$

The solving of Equation 1.69 brings the solution of the temperature field for the unsteady two-dimensional heat conduction. The evolution of temperature can be observed by recording the node temperature at each time level, and the heating (or cooling) curves at special points can also be extracted from the result files.

1.3.3 FEM for Three-Dimensional Unsteady Heat Conduction

The principles and procedure in the FEM for three-dimensional unsteady heat conduction are identical to those in the two-dimensional one, as presented in the previous section. The derivation of its FEM formulations is more complex and can be found in related monographs [5–7]. Here, only the derived results are briefly outlined.

The governing PDE of three-dimensional unsteady heat conduction with an internal heat resource is repeated here.

$$\lambda\left(\frac{\partial^2 T}{\partial x^2} + \frac{\partial^2 T}{\partial y^2} + \frac{\partial^2 T}{\partial z^2}\right) + Q = \rho c_p \frac{\partial T}{\partial \tau} \tag{1.70}$$

Supposing that there are total n elements (m nodes in each element) and p nodes after the discretization of the whole solution domain, Equation 1.70 can be transformed into an algebraic equation group as follows:

$$[K]\{T\} + [C]\left\{\frac{\partial T}{\partial \tau}\right\} - \{P\} = 0 \tag{1.71}$$

$$[K] = \sum [K]^{e} \tag{1.71a}$$

$$[C] = \sum [C]^{e} \tag{1.71b}$$

$$\{P\} = \sum \{P\}^{e} \tag{1.71c}$$

$$[K]^{e} = \iiint_{V^e} [B]^{T}[D][B]\mathrm{d}v + \iint_{S^e} h[N]^{T}[N]\mathrm{d}s \tag{1.71d}$$

$$[C]^{\mathrm{e}} = \iiint_{V^{\mathrm{e}}} \rho c_p [N]^{\mathrm{T}} [N] \mathrm{d}v \tag{1.71e}$$

$$[p]^{\mathrm{e}} = \iiint_{V^{\mathrm{e}}} Q[N]^{\mathrm{T}} \mathrm{d}v + \iint_{S^{\mathrm{e}}} hT_{\mathrm{a}}[N]^{\mathrm{T}} \mathrm{d}s \tag{1.71f}$$

$$[D] = \begin{bmatrix} \lambda & 0 & 0 \\ 0 & \lambda & 0 \\ 0 & 0 & \lambda \end{bmatrix} \tag{1.71g}$$

$$[B] = \begin{bmatrix} \dfrac{\partial N_1}{\partial x} & \dfrac{\partial N_2}{\partial x} & \cdots & \dfrac{\partial N_P}{\partial x} \\ \dfrac{\partial N_1}{\partial y} & \dfrac{\partial N_2}{\partial y} & \cdots & \dfrac{\partial N_P}{\partial y} \\ \dfrac{\partial N_1}{\partial z} & \dfrac{\partial N_2}{\partial z} & \cdots & \dfrac{\partial N_P}{\partial z} \end{bmatrix} \tag{1.71h}$$

$$[N] = [N_1 N_2 \cdots N_P] \tag{1.71i}$$

where

V^{e} is the element volume

S^{e} is the exterior boundaries

In the unsteady temperature field, the variable temperature $T_{(x,y,z,\tau)}$ is a function of spatial location and time. Equation 1.71 is the spatial discretized formulation with the time differential item $\partial T/\partial \tau$, which can be discretized by the difference method in a uniform format as follows:

$$\theta \left(\frac{\partial T}{\partial \tau}\right)_{\tau} + (1-\theta)\left(\frac{\partial T}{\partial \tau}\right)_{\tau-\Delta\tau} = \frac{1}{\Delta \tau}(T_{\tau} - T_{\tau-\Delta\tau}) \tag{1.72}$$

If $\theta = 1$, the backward difference format of time discretization is

$$\left(\frac{\partial T}{\partial \tau}\right)_{\tau} = \frac{1}{\Delta \tau}(T_{\tau} - T_{\tau-\Delta\tau}) \tag{1.73}$$

Substituting Equation 1.73 into Equation 1.71, we get

$$\left([K] + \frac{1}{\Delta \tau}[C]\right)\{T_{\tau}\} = \frac{1}{\Delta \tau}[C]\{T_{\tau-\Delta\tau}\} + \{P\} \tag{1.74}$$

If $\theta = 1/2$, the Crank–Nicolson difference format (also named central difference format) of time discretization can be obtained as

$$\frac{1}{2}\left[\left(\frac{\partial T}{\partial \tau}\right)_{\tau} + \left(\frac{\partial T}{\partial \tau}\right)_{\tau-\Delta\tau}\right] = \frac{1}{\Delta \tau}(T_{\tau} - T_{\tau-\Delta\tau}) \tag{1.75}$$

Substituting Equation 1.75 into Equation 1.71, the corresponding FEM algebraic equation can be obtained as follows:

$$\left([K] + \frac{2}{\Delta \tau}[C]\right)\{T_{\tau}\} = \left(\frac{2}{\Delta \tau}[C] - [K]\right)\{T_{\tau-\Delta\tau}\} + \frac{1}{\Delta \tau}(\{P\}_{\tau} + \{P\}_{\tau-\Delta\tau}) \tag{1.76}$$

The Crank–Nicolson difference format is, in general, more accurate than the backward difference method, in that it does not give preference to either temperature at time level $\tau - \Delta\tau$ or time level τ but, rather, gives equal credence to both.

In FDM of time, the key parameter governing solution accuracy is the selected time step $\Delta\tau$. In a fashion similar to the FEM, in which the smaller the elements are, physically, the better is the solution, the FDM converges more rapidly to the true solution as the time step is decreased.

When the temperature field at time level $\tau - \Delta\tau$ is known, and input into Equation 1.74 or Equation 1.76, the temperature $\{T_\tau\}$ on all nodes at time level τ can thus be solved, and the marching solution can progress in time until a steady state is reached. The nodal temperatures, recorded step by step at different time levels, constitute the evolution history of the three-dimensional temperature field.

1.4 CALCULATION OF TRANSFORMATION VOLUME FRACTION

1.4.1 Interactions between Phase Transformation and Temperature

The latent heat releases as an internal heat source inside the solid when phase transformation occurs. Thus, the kinetics of phase transformation strongly depends on the temperature history of steel parts, but also strongly affects the temperature field inside. The interactions between phase transformation and temperature are not one-way, but bilateral, increasing the complexity in the accurate numerical simulation of the thermal processing.

The latent heat per time unit, expressed as the internal heat source in the heat conduction equation, i.e., Equation 1.1, is usually calculated by the following Equation 1.77:

$$Q = \Delta H \frac{\Delta V}{\Delta \tau} \tag{1.77}$$

where

ΔH is the enthalpy difference when a new phase of unit volume forms from the parent phase
ΔV is the change of transformation fraction in the time step $\Delta\tau$

The calculation of the volume fraction is the key to predict the evolution of temperature and microstructure during the thermal processing, as well as the final microstructure constituents and rough mechanical property. Since phase transformations are usually classified into two categories according to their mechanisms, diffusion transformation (for example, pearlite transformation), and nondiffusion transformation, i.e., martensitic transformation, the mathematical models of the transformation kinetics are very different.

In this section, the numerical method to calculate the transformed volume fraction of a new phase is mainly introduced.

1.4.2 Diffusion Phase Transformation

A time–temperature–transformation (TTT) diagram describes the relationship between the transformation starting, ending, and the transformed volume fraction during the isothermal process at different temperatures. The isothermal kinetics equation, namely Johnson–Mehl equation [8], provides a solid base for numerical simulation of thermal process although it cannot be directly applied to calculate the volume fraction due to the nonisothermal process of the practical heating or cooling process. Until now, the method proposed by Fernandes et al. [9] has been widely accepted, in which the practical nonisothermal process is considered as many isothermal stages with a tiny time duration as shown in Figure 1.5, and the effect of these stages can be summed together according to Scheil's additivity rule.

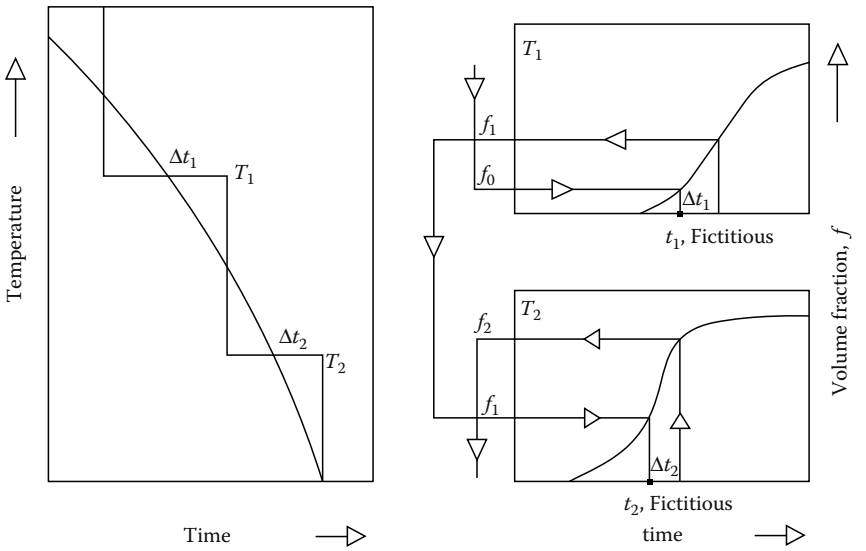

FIGURE 1.5 Schematic model for fraction calculation of diffusion transformation during continuous cooling process.

Due to the strict limits of Johnson–Mehl equation, Avrami [10] proposed an empirical equation, which has a simpler form and has been widely used, as follows:

$$f = 1 - \exp(-bt^n) \tag{1.78}$$

where

f is the volume fraction of a new phase
t is the isothermal time duration
b is a constant dependent on the temperature, composition of parent phase, and the grain size
n is also a constant dependent on the type of phase transformation and ranges from 1 to 4

Coefficient b and n at different temperatures are usually calculated from the experimentally obtained TTT diagrams by the following equations:

$$n_{(T)} = \frac{\ln[\ln(1-f_1) - \ln(1-f_2)]}{\ln t_1 - \ln t_2} \tag{1.79}$$

$$b_{(T)} = \frac{\ln(1-f_1)}{t_1^{n(T)}} \tag{1.80}$$

Therefore, the relationship between the volume fraction and time under certain isothermal temperatures can be calculated by Equations 1.78 through 1.80. Most experimental data of phase transformation agree well with the Avrami equation.

Only with the help of Scheil's additivity rule can the transformation starting time, namely, the incubation period, for a nonisothermal cooling or heating process be determined. The general form of Scheil's additivity rule can be written as

$$\int_0^{t_s} \frac{\mathrm{d}t}{t_i^{\mathrm{TTT}}} = 1 \quad \text{or} \quad \sum_{i=1}^{n} \frac{\Delta t_i}{t_i^{\mathrm{TTT}}} = 1 \tag{1.81}$$

where

t_s is the incubation period to be determined for the nonthermal process
t_i^{TTT} is the incubation period under a certain isothermal temperature
Δt_i is the time step

It can be understood that the transformation in the nonisothermal process occurs when the summation of the relative fractions $\Delta t_i / t_i^{TTT}$ reaches unity.

Scheil's additivity rule has also been applied in volume fraction calculation. For example, to find the time (t_m) needed to attain a certain fraction transformed (ξ_m) in a nonisothermal transformation with time–temperature path T_t, Scheil's additivity rule is expressed as

$$\int_0^{t_m} \frac{dt}{t_{\xi_m}(T)} = 1 \tag{1.82}$$

where $t_{\xi_m}(T)$ is the time to transform the fraction ξ_m isothermally at the current isotherm T_t. According to Equation 1.82, the total time required for completion of the transformation is obtained by adding the absolute durations of time Δt spent at each temperature T, until the sum of the relative durations $\Delta t / t_{\xi_m}(T)$ becomes unity. The time $t_{\xi_m}(T)$, to reach transformed fraction ξ_m, can be obtained from the kinetics equation, i.e., the Avrami equation (Equation 1.78).

To explicitly demonstrate its calculation method, the concept of fictitious time t^* and fictitious transformed volume fraction f_i^* are commonly developed [9]. These two variables can be calculated by

$$t_i^* = \left[\frac{-\ln(-f_{i-1})}{b_i}\right]^{1/n_i} \tag{1.83}$$

$$f_i^* = 1 - \exp[b_i(t_i^* + \Delta t)^{n_i}] \tag{1.84}$$

Hence, the practical transformed fraction is

$$f = f_i^*\left(f_{i-1}^{\gamma} + f_{i-1}\right) f_{\max} \tag{1.85}$$

where

f_{i-1}^{γ} and f_{i-1} are the austenite fraction and transformed fraction at the end of the previous time step
$f_{\max}$ is the maximum possible transformed fraction for this type of transformation

Equations 1.78 through 1.85 constitute the basic frame of volume fraction calculation for the diffusion transformation, whereas it should be carefully applied in specific case studies and necessary modifications be made.

1.4.2.1 Modification of Additivity Rule for Incubation Period

Based on theoretical analysis and experimental results, Hsu [11] points out that the additivity rule is not always accurate enough to be applicable in incubation period prediction. Hawbolt et al. [12] and Reti and Felde [13] held the same viewpoint that the additivity rule sometimes seriously overestimates the incubation time.

Taking the eutectoid steel as the example, the practical incubation period t_s^{CCT} under certain cooling rate, as well as the incubation periods for different isothermal stages t_s^{TTT}, can be obtained

TABLE 1.1
Summation of Relative Durations in Nonisothermal Process of Eutectoid Steel

Average Cooling Rate, °C/s	Summation of Relative Durations, χ	Source
7.5	0.2	[12]
2.0	0.23	
38.5	0.24	
5.3	0.43	[14]
21.2	0.31	
47.6	0.28	

from CCT and TTT diagrams, respectively. Hence, the relative durations of each tiny isothermal stage $\Delta t/t_s^{TTT}$ can be summed stage by stage from zero to t_s^{CCT} by

$$\chi = \sum_{0}^{t_s^{CCT}} \frac{\Delta t}{t_s^{TTT}} \tag{1.86}$$

Beyond expectation, the summation χ, listed in Table 1.1, is much less than unity.

Another approach has been proposed to modify the additivity rule for prediction of incubation period using TTT and CCT diagrams simultaneously [14].

The starting curves of TTT and CCT diagram are plotted together as Figure 1.6. The average cooling rate during arbitrary time step Δt_i on the practical cooling curve, that is, the slope of the tangent line dd drawn at the middle point of time step Δt_i, can be calculated by

$$V_i = \frac{T_{i-1} - T_i}{\Delta t_i} \tag{1.87}$$

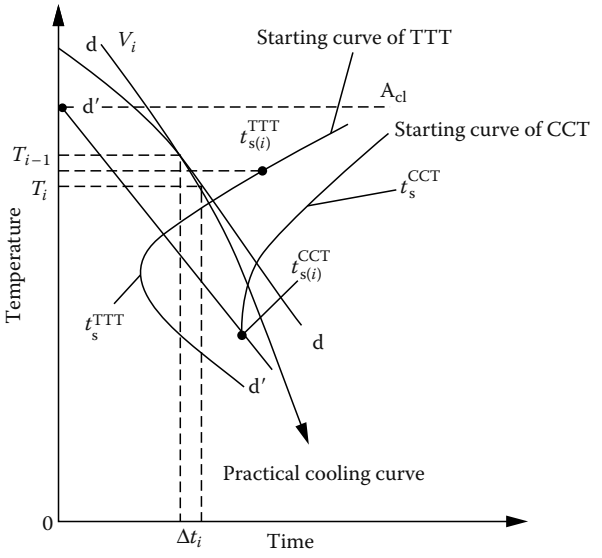

FIGURE 1.6 Schematic sketch of the modification of additivity rule for incubation period.

Cooling from the critical point A_{c1} with the constant rate of V_i, the cross point with the starting curve t_s^{CCT} in the CCT diagram gives the incubation period $t_{s(i)}^{CCT}$, during which the modification coefficient φ_i of relative durations in this time step for the TTT diagram can be calculated by

$$\varphi_i = \int_0^{t_{s(i)}^{CCT}} \frac{dt}{t_s^{TTT}} \tag{1.88}$$

The modification coefficient φ_i reflects the difference in incubation period between the CCT and TTT diagram. When φ_i equals unity, there is no difference. Usually, it is bigger than unity since it is very common that the starting curve in CCT lags behind that in the TTT diagram. Therefore, the relative time duration $\Delta t_i / t_{s(i)}^{TTT}$ for the time step Δt_i can be modified as $(\Delta t_i / t_{s(i)}^{TTT})(1/\phi_i)$.

Hence, for the transformation starting time, namely, the incubation period for the isothermal process, the criterion is modified as follows:

$$\sum \frac{\Delta t_i}{t_{s(i)}^{TTT}} \times \frac{1}{\varphi_i} = 1 \tag{1.89}$$

The theoretical derivation of this modification is still in the process of consummation, and the application and the accuracy also need to be further validated.

1.4.2.2 Modification of Avrami Equation

It is very clear that the time in the Avrami Equation 1.78 counts since the transformation occurs, that is, the incubation period is not included. Therefore, Hawbolt et al. [12] suggested that the modified form of Avrami equation should be

$$f = 1 - \exp[-b(t - t_s)^n] \tag{1.90}$$

The calculation of coefficients n and b is also changed as

$$n(T) = \frac{\ln[\ln(1 - f_1) - \ln(1 - f_2)]}{\ln(t_1 - t_s) - \ln(t_2 - t_s)} \tag{1.91}$$

$$b(T) = \frac{\ln(1 - f_1)}{(t_1 - t_s)^{n(T)}} \tag{1.92}$$

where t_s is the incubation period of the isothermal process at a certain temperature.

To demonstrate the difference between these two methods, again, the eutectoid steel (T8 steel) is taken as an example. In the algorithm 1 based on the Avrami equation, the transformation starting time t_s (approximate as $t_{0.01}$) and ending time t_e (approximate as $t_{0.99}$) read from the TTT diagram are input to Equations 1.78 through 1.80 to calculate the coefficients n, b, and $t_{0.25}$ (the time needed to get a fraction of 0.25 of the new phase). In the algorithm 2 based on the modified Avrami equation, $t_{0.5}$ and $t_{0.75}$ are the time to transform the new phase of the volume fraction of 0.5 and 0.75, respectively, both of which include the incubation period t_s and can be got from the TTT diagram. With the help of Equations 1.90 through 1.92, the coefficients n, b, and $t_{0.25}$ are also calculated. All these data are listed in Table 1.2. It is obvious that the modified Avrami equation seems more reasonable and fits better with the TTT diagram than the unmodified one.

TABLE 1.2
Coefficients *n*, *b*, and $t_{0.25}$ Calculated by Different Methods

Temperature (°C)	Data from TTT Diagram of Eutectoid Steel (T8 Steel)					Algorithm 1: Avrami Equation			Algorithm 2: Modified Avrami Equation		
	t_s (s)	$t_{0.25}$ (s)	$t_{0.5}$ (s)	$t_{0.75}$ (s)	t_e (s)	$n(T)$	$b(T) \times 10^{-5}$	$t_{0.25}$ (s)	$n(T)$	$b(T) \times 10^{-5}$	$t_{0.25}$ (s)
700	12.5	39	63	90	120	2.71	1.07	43.1	1.62	121	41.9
650	2.7	6.5	8.8	11.5	18.5	3.18	42.5	7.7	1.89	2271	6.5
450	1.4	5.5	8.0	11	20	2.13	463	6	2.05	1460	5.7
400	3	30	4.3	65	100	1.75	147	20.5	1.58	200	26

1.4.2.3 Calculation of Proeutectoid Ferrite and Pearlite Fraction

The transformations in the hypoeutectoid steel can be explained by Figure 1.7. When the steel is cooled rapidly until the temperature is below line SE′, the stable ferrite α and cementite Fe_3C precipitate simultaneously and form the quasieutectoid. However, if the temperature is above point a, for example, at point a′, the nucleus of ferrite appears first at the austenite grain boundary, and the ferrite grows up as the time goes on. At the same time, carbon diffuses into the neighboring austenite grain due to its low dissolvability in ferrite, increasing the carbon concentration in austenite. When the concentration reaches point b located on the boundary of two-phase area $\alpha + Fe_3C$, the retained austenite starts to decompose into pearlite.

The mechanism of the transformation process has been investigated intensively and has almost reached common understanding, while the fraction calculation of proeutectoid ferrite and pearlite is an unsettled dispute.

The nucleation sites and the mode of the proeutectoid ferrite are theoretically different from those of eutectoid pearlite. Although their growth is controlled by diffusion, the growth mode and diffusion route of carbon are different. These factors support the viewpoint that the fraction of proeutectoid ferrite and pearlite should be calculated separately, that is, two sets of independent

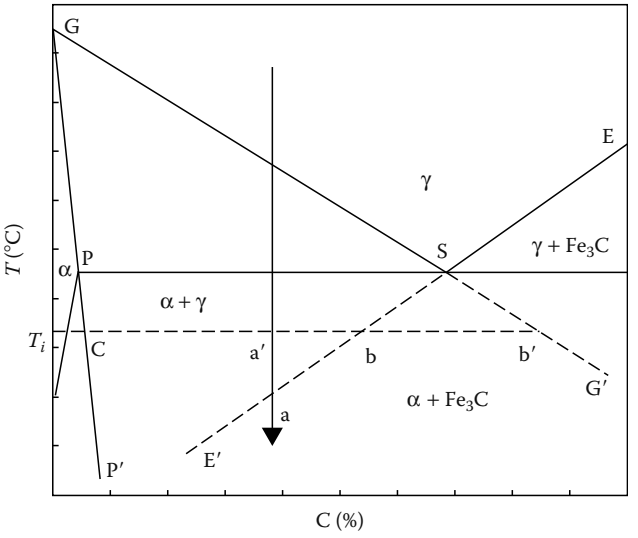

FIGURE 1.7 Schematic sketch of the quasiequilibrium diagram of Fe-C.

Avrami equations should be used. Therefore, Wang et al. [15] proposed that the volume fraction of proeutectoid ferrite and pearlite in steel 1025 be calculated by two Avrami equations as

$$f_{\mathrm{F}} = 1 - \exp[-b_{\mathrm{F}}(t - t_{\mathrm{SF}})^{n_{\mathrm{F}}}] \tag{1.93}$$

$$f_{\mathrm{P}} = 1 - \exp[-b_{\mathrm{P}}(t - t_{\mathrm{SP}})^{n_{\mathrm{P}}}] \tag{1.94}$$

On the other hand, the proeutectoid ferrite precipitates along the austenite grain boundary, and there is enough space for growth at the initial stage. However, with the growth of the new phase, the volume fraction increases, and the transformation rate decreases because of the encounter of the new phase. Usually, the pearlite transformation occurs when the proeutectoid ferrite precipitation is still in process. Hence, the proposal [12,15] that the proeutectoid ferrite precipitation should be described by one dependent Avrami equation seems to lack convincing evidence.

In addition, the starting temperature of pearlite transformation during continuous cooling is hard to determine because the carbon content of austenite varies with the precipitation of proeutectoid ferrite. The pearlite transformed is usually the quasi-eutectoid in which the carbon content decreases with the decrease in temperature. These are not in agreement with the hypotheses of the additivity rule.

Based on the above analysis, Pan et al. [16] developed a set of new approaches that uses one combined Avrami equation to calculate the total volume fraction of proeutectoid ferrite and pearlite. Assuming that the steel is isothermally kept for enough long time to precipitate the proeutectoid ferrite only and the pearlite transformation does not occur, the final volume fraction of ferrite $f_{\mathrm{end}}^{\mathrm{F}}$ under certain temperature T_i can be calculated by lever rule as

$$f_{\mathrm{end}}^{\mathrm{F}} = \frac{a'b'}{cb'} \tag{1.95}$$

Therefore, the definition domain of the Avrami equation describing the proeutectoid ferrite is $[0, f_{\mathrm{end}}^{\mathrm{F}}]$. However, the practical situation is that the pearlite transformation usually occurs before the volume fraction of proeutectoid ferrite reaches $f_{\mathrm{end}}^{\mathrm{F}}$. Thus, there exists a maximum volume fraction of proeutectoid ferrite $f_{\mathrm{max}}^{\mathrm{F}}$ at a certain temperature, which can be calculated as

$$f_{\mathrm{max}}^{\mathrm{F}} = \frac{ba'}{cb} \tag{1.96}$$

When the volume fraction of proeutectoid ferrite reaches $f_{\mathrm{max}}^{\mathrm{F}}$, the carbon concentration in the retained austenite reaches the composition range of quasieutectoid. The decomposition of austenite enters the stage of pearlite transformation. The accurate kinetics of austenite decomposition, i.e., the solid line in Figure 1.8, can be split into two parts: the first part is the transformation of proeutectoid ferrite from $[0, f_{\mathrm{max}}^{\mathrm{F}}]$, and the second part is that of pearlite from $[f_{\mathrm{max}}^{\mathrm{F}},1]$. The whole curve is still S type and can be united into one Avrami equation.

The total volume fraction of proeutectoid ferrite f_{F_i} and pearlite f_{P_i} can be calculated referring to previous sections, and their separation is performed:

$$\text{If } f_i < f_{\mathrm{max}}^{\mathrm{F}}, \quad \text{then } \begin{cases} f_{\mathrm{F}_i} = f_i \\ f_{\mathrm{P}_i} = 0 \end{cases} \tag{1.97}$$

$$\text{If } f_i \geq f_{\mathrm{max}}^{\mathrm{F}}, \quad \text{then } \begin{cases} f_{\mathrm{F}_i} = f_{\mathrm{max}}^{\mathrm{F}} \\ f_{\mathrm{P}_i} = f_i - f_{\mathrm{max}}^{\mathrm{F}} \end{cases} \tag{1.98}$$

In order to test this approach, the TTT and CCT diagram of 45# steel was used to calculate the volume fraction of proeutectoid ferrite f_{F_i} and pearlite f_{P_i}, which were then input into the additivity rule as

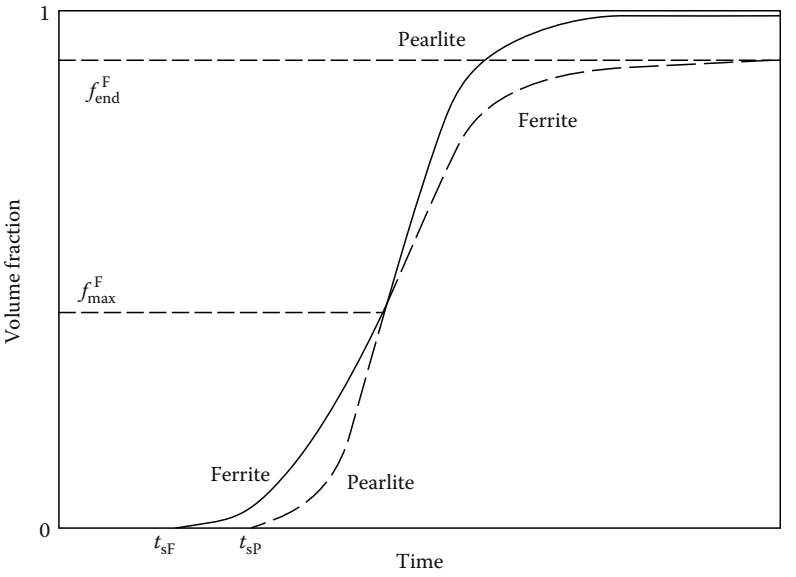

FIGURE 1.8 Schematic sketch of isothermal transformation in hypoeutectoid steel.

TABLE 1.3
Results of Check Computation of the Additivity Rule in 45# Steel

Average Cooling Rate (°C/s)	t_s^{CCT} (s)	t_s^{CCT} (°C)	t_e^{TTT} (s)	x_i
0.6	113.3	717	288.3	0.98
8.1	9.5	689	635	0.97
25	2.7	670	625	0.94

$$x_i = \sum_{t_s^{CCT}}^{t_e^{CCT}} \frac{\Delta t_i}{t_{ei}^{TTT} - t_{si}^{TTT}} \tag{1.99}$$

The results listed in Table 1.3 indicate that the summation of relative durations almost reaches unity under different cooling rates, demonstrating the feasibility of the approach discussed here.

Related experimental and simulation results [17] also demonstrated that the whole decomposition process of austenite in hypoeutectoid steel can be reasonably described by one Avrami equation.

1.4.3 Martensitic Transformation

In most cases, the transformed volume fraction of martensite is independent of the cooling rate, but a function of temperature. The Koistinen–Marburger [18] equation is always adopted in thermal process simulation, and it is

$$f_M = 1 - \exp[-\alpha(M_s - T)] \tag{1.100}$$

where

f_M is the transformed volume fraction of martensite
T is the temperature
M_s is the start temperature of martensitic transformation
α is the constant reflecting the transformation rate and varying with the steel composition

For carbon steel with the carbon content lower than 1.1%, we have $\alpha = 0.011$.

Assuming that the average volume of martensite lamella is constant, Magee [19] theoretically derived the constant α as

$$\alpha = \overline{V}\varphi \frac{\partial \Delta G_v^{\gamma \to M}}{\partial T} \tag{1.101}$$

where

$\overline{V}$ is the average volume of martensite lamella
φ is the ratio of the martensite number newly formed to the driving force in the austenite of unit volume
$\Delta G_v^{\gamma \to M}$ is the free energy difference between austenite and martensite

Hsu [20] inferred that the Koistinen–Marburger equation is only applicable in high and medium carbon content steels in which the carbon does not diffuse when martensite transform occurs. While in the low carbon steel and the medium carbon steel with strip austenite the alloy element affects the carbon diffusion. Therefore, the Koistinen–Marburger equation should be modified for the low carbon steel, and it becomes

$$f = 1 - \exp\left[\beta(C_1 - C_0) - \alpha(M_s - T_q)\right] \tag{1.102}$$

where

C_0 is the carbon concentration in austenite
C_1 is the carbon concentration in martensite

α and β are constants dependent on the materials; the former can be obtained according to Equation 1.101, while the latter can be calculated as follows:

$$\beta = \overline{V}\varphi \frac{\partial \Delta G_v^{\gamma \to M}}{\partial C} \tag{1.103}$$

where C is the carbon concentration.

Generally, the volume of martensite in the carbon steel and alloy steel is calculated using Equations 1.100 and 1.102, and the M_s point can be obtained by experiment and the following empirical equations:

$$M_s(^\circ\mathrm{C}) = 520 - (C\%) \times 320 \tag{1.104}$$

$$\begin{aligned} M_s(^\circ\mathrm{C}) = {} & 512 - 453\mathrm{C} - 16.9\mathrm{Ni} + 15\mathrm{Cr} - 9.5\mathrm{Mo} + 217(\mathrm{C})^2 \\ & - 71.5(\mathrm{C})(\mathrm{Mn}) - 67.6(\mathrm{C})(\mathrm{Cr}) \end{aligned} \tag{1.105}$$

The M_s point is considered as a constant in Koistinen–Marburger equation, while it varies if other transformations, for example, pearlite transformation, bainite transformation, and so on, occur heretofore, changing the composition of the parent phase or consuming the embryos. It can be

observed from the CCT curves that the more the austenite decomposes, the more the M_s point decreases. The phenomenon has not been generally reflected in the additivity rule in calculation of volume fractions using TTT curves. Hence, the calculation model, i.e., the Koistinen–Marburger equation, for martensite is in great need of further amendment based on transformation mechanisms to improve its universality and accuracy.

1.4.4 Effect of Stress State on Phase Transformation Kinetics

The stress state has considerable effects on the phase transformation kinetics irrespective of the diffusion transformation or that of nondiffusion. Numerous investigations [21–25] have been carried out to clarify the mechanism and to establish effective models for accurate simulation. Up to now, the research in this field is still far from satisfactory. Some mathematical models proposed by different groups are only applicable for some specific steels, and some need to be further validated. In this section, representative models are briefly introduced.

1.4.4.1 Diffusion Transformation

For the pearlite transformation, Inoue and Wang [26] developed the model of transformation kinetics under stress. In his work, the Johnson–Mehl equation in the stress-free state is expressed as

$$f = 1 - \exp\left(-\int_0^t F(T)(t-\tau)^3 \mathrm{d}\tau\right) \tag{1.106}$$

The Johnson–Mehl equation under stress state was modified as

$$f = 1 - \exp\left(-\int_0^t \exp(c\sigma_m) F(T)(t-\tau)^3 \mathrm{d}\tau\right) \tag{1.107}$$

where
$F(T)$ is the temperature function
σ_m is the mean stress
c is a constant

Denis et al. [27] introduced the effect of stress into the coefficients (n and b) in the Avrami equation (Equation 1.78) as follows:

$$n_\sigma = n \tag{1.108}$$

$$b_\sigma = \frac{b}{(1 - C\sigma_e)^n} \tag{1.109}$$

where
σ_e is the equivalent stress
C is a constant

1.4.4.2 Martensitic Transformation

For martensitic transformation, the stress state in the steel has much greater effects on the transformation process. The coefficient α in the Koistinen–Marburger equation (Equation 1.100), as well as the M_s point, is strongly dependent on the stress state.

Observing Equation 1.101, the coefficient α can be obtained from the driving force in which the stress plays an important role. Thus, Hsu proposed an empirical equation as follows, indicating the relationship between α and equivalent stress σ_{i}.

$$\alpha = \alpha_0 + \alpha_1 \sigma_{\mathrm{i}} \tag{1.110}$$

where the coefficients are about $\alpha_0 = 1.2430 \times 10^{-2}$ and $\alpha_1 = 6.9752$.

Inoue and Wang [26] expressed the Koistinen–Marburger equation without stress as

$$f = 1 - \exp(\phi(T)) \tag{1.111}$$

while the kinetics equation under stress was modified as

$$f = 1 - \exp\left[\left(A\sigma_{\mathrm{m}} + BJ_2^{\frac{1}{2}}\right) + \phi(T)\right] \tag{1.112}$$

where

σ_{m} is the mean stress, i.e., hydrostatic pressure
J_2 is the second stress invariant
coefficients A and B are the material constants

Similarly, Denis et al. [27] developed the model of martensitic transformation under stress, and her equation for volume fraction of martensite is

$$f = 1 - \exp\left(-\alpha(M_{\mathrm{s}} + A\sigma_{\mathrm{m}} + B\sigma_{\mathrm{i}} - T) + \left(A\sigma_{\mathrm{m}} + B\sigma_{\mathrm{i}}^{1/2}\right)\right) \tag{1.113}$$

Compared to Equation 1.112, this equation additionally considers the effect of stress on the M_{s} point, which can be clearly expressed as an extra item ΔM_{s} [28]. Therefore, we have

$$M_{\mathrm{s}}^{\sigma} = M_{\mathrm{s}} + \Delta M_{\mathrm{s}} \tag{1.114}$$

$$\Delta M_{\mathrm{s}} = A\sigma_{\mathrm{m}} + B\sigma_{\mathrm{i}} \tag{1.115}$$

1.5 CONSTITUTIVE EQUATION OF SOLIDS

1.5.1 Elastic Constitutive Equation

1.5.1.1 Linear Elastic Constitutive Equation

In a solid under deformation, the stress depends on the current strain state, and is a single value function of the strain. The elastic deformation will be recovered, when the load is released, i.e., the elastic deformation is reversible. Usually elastic constitutive relation is taken as linear.

1.5.1.1.1 Isotropic Elasticity

In the isothermal, small deformation process of solids, the stress components are a linear function of the components of the small strain tensor, as follows:

$$\sigma_{ij} = C_{ijkl}^{\mathrm{e}} \varepsilon_{kl}^{\mathrm{e}} \tag{1.116}$$

where C_{ijkl}^{e} is the elastic tensor, the superscript "e" means elastic

Such a material model is called linear elastic constitutive equation. The incremental form of the above equation is

$$\mathrm{d}\sigma_{ij} = C^{\mathrm{e}}_{ijkl}\,\mathrm{d}\varepsilon^{\mathrm{e}}_{kl} \tag{1.117}$$

Usually metals can be taken as isotropic, linear elastic materials or ideal elastic materials. For such materials, the elastic tensor is a fourth-order isotropic tensor, including only two independent parameters, as follows:

$$C^{\mathrm{e}}_{ijkl} = 2G\left(\delta_{ik}\delta_{jl} + \frac{\nu}{1-2\nu}\delta_{ij}\delta_{kl}\right) \tag{1.118}$$

where

G is the shear modulus
ν is the Poisson's ratio

G is related with Young's modulus E by the following equation:

$$G = \frac{E}{2(1+\nu)}$$

In finite deformation, to meet the requirement of objectivity, the Jaumann rate of Cauchy stress tensor and the rate of deformation tensor, which possess objectivity, are adopted, and the elastic constitutive equation is rewritten as

$$\hat{\sigma}_{ij} = C^{\mathrm{e}}_{ijkl} d^{\mathrm{e}}_{kl} \tag{1.119}$$

For the convenience of finite-element formulation, the stress and strain are usually rewritten from second-order tensors into vectors, e.g.,

$$\boldsymbol{\sigma} = [\sigma_{11}\sigma_{22}\sigma_{33}\sigma_{12}\sigma_{23}\sigma_{31}]^{\mathrm{T}}$$
$$\boldsymbol{\varepsilon} = [\varepsilon_{11}\varepsilon_{22}\varepsilon_{33}2\varepsilon_{12}2\varepsilon_{23}2\varepsilon_{31}]^{\mathrm{T}}$$

Accordingly, the fourth-order tensor C^{e} is rewritten into a matrix:

$$\mathbf{C}^{\mathrm{e}} = \frac{2G}{1-2\nu}\begin{bmatrix} 1-\nu & \nu & \nu & 0 & 0 & 0 \\ \nu & 1-\nu & \nu & 0 & 0 & 0 \\ \nu & \nu & 1-\nu & 0 & 0 & 0 \\ 0 & 0 & 0 & (1-2\nu)/2 & 0 & 0 \\ 0 & 0 & 0 & 0 & (1-2\nu)/2 & 0 \\ 0 & 0 & 0 & 0 & 0 & (1-2\nu)/2 \end{bmatrix} \tag{1.120}$$

Then the elastic constitutive equation can be written in the matrix form:

$$\boldsymbol{\sigma} = \mathbf{C}^{\mathrm{e}}\boldsymbol{\varepsilon}$$

In this chapter, the symbol σ is used to represent the stress both in tensorial form and in vectorial form. Similar usage is also applied for $\boldsymbol{\varepsilon}$ and $\mathbf{C}^{\mathrm{e}}$. The exact meaning of the symbol can be deduced from the context.

Elastic deformation can be decomposed into a volumetric component,

$$\varepsilon_m^{\mathrm{e}} = \left(\varepsilon_{11}^{\mathrm{e}} + \varepsilon_{22}^{\mathrm{e}} + \varepsilon_{33}^{\mathrm{e}}\right)/3$$
$$\varepsilon_{ij}^{\mathrm{e}'} = \varepsilon_{ij}^{\mathrm{e}} - \varepsilon_m^{\mathrm{e}}\delta_{ij}$$
$$\varepsilon_{ij}^{\mathrm{e}'} = \frac{1}{2G}\sigma_{ij}'$$
$$\varepsilon_m^{\mathrm{e}} = \frac{1-2\nu}{E}\sigma_m$$

1.5.1.1.2 Orthotropic Elasticity

Some materials, such as a single crystal, show different elastic behavior along different directions. If the principal axes are mutually orthogonal, it is called orthotropic elasticity. If along each principal axis, the elastic properties are identical, then the elastic matrix is

$$\mathbf{C}^{\mathrm{e}} = \begin{bmatrix} C_{11} & C_{12} & C_{12} & 0 & 0 & 0 \\ C_{12} & C_{11} & C_{12} & 0 & 0 & 0 \\ C_{12} & C_{12} & C_{11} & 0 & 0 & 0 \\ 0 & 0 & 0 & C_{44} & 0 & 0 \\ 0 & 0 & 0 & 0 & C_{44} & 0 \\ 0 & 0 & 0 & 0 & 0 & C_{44} \end{bmatrix} \tag{1.121}$$

1.5.1.2 Hyperelastic Constitutive Equation

Some materials such as rubbers, have highly nonlinear stress–train relationships; they remain elastic even when they go through a huge deformation. Such materials are described by hyperelastic constitutive equation.

If a material possesses the strain energy density function, w, which is an analytic function of the strain tensor, and the increment of which is the work done by the stress, then it is called hyperelastic material. For hyperelastic material

$$w = \frac{1}{\rho_0} S_{ij}\dot{E}_{ij} \tag{1.122}$$

where

ρ_0 is the mass density in initial configuration
S_{ij} is the second Piola–Kirchhoff stress tensor
$\dot{E}_{ij}$ is the Green strain tensor

On the other hand, the strain energy function is the analytic function of strain tensor; then

$$\dot{w} = \frac{\partial w}{\partial E_{ij}}\dot{E}_{ij} \tag{1.123}$$

$$\left(\frac{1}{\rho_0} S_{ij} - \frac{\partial w}{\partial E_{ij}}\right)\dot{E}_{ij} = 0 \tag{1.124}$$

If the components of $\dot{E}_{ij}$ are mutually independent, from the arbitrariness of $\dot{E}_{ij}$, we have

$$S_{ij} = \rho_0 \frac{\partial w}{\partial E_{ij}} \tag{1.125}$$

Equation 1.125 is the hyperelastic constitutive equation.

If the volume change in deformation process is negligible, then the components of $\dot{E}_{ij}$ are not independent, but should meet the incompressible condition:

$$\varepsilon_{ii} = \frac{\partial X_m}{\partial x_i} \frac{\partial X_n}{\partial x_i} \dot{E}_{mn} = 0 \tag{1.126}$$

Comparing Equations 1.124 and 1.126, it is known that

$$\frac{1}{\rho_0} S_{ij} - \frac{\partial w}{\partial E_{ij}} = \frac{\partial X_i}{\partial x_m} \frac{\partial X_j}{\partial x_m}$$

That is,

$$S_{ij} = \frac{1}{\rho_0} \frac{\partial w}{\partial E_{ij}} + h \frac{\partial X_m}{\partial x_i} \frac{\partial X_n}{\partial x_i} \tag{1.127}$$

where h is the hydrostatic pressure, determined by the boundary conditions. Equation 1.127 is the constitutive equation of incompressible hyperelastic materials.

For isotropic hyperelastic materials, the deformation energy density function could be expressed as a function of the invariables of Green deformation tensor:

$$w = w(I_1, I_2, I_3)$$

where

$$\left.\begin{aligned} I_1 &= C_{ii} = 2E_{ii} + 3 \\ I_2 &= \left(C_{ii}C_{jj} - C_{ij}C_{ji}\right)/2 = 2E_{ii}E_{jj} + 4E_{ii} - 2E_{ij}E_{ij} + 3 \\ I_3 &= \det \mathbf{C} = \det\left(\frac{\partial x_m}{\partial X_i} \frac{\partial x_m}{\partial X_j}\right) \end{aligned}\right\} \tag{1.128}$$

So

$$S_{ij} = \rho_0 \left[\frac{\partial w}{\partial I_1} \frac{\partial I_1}{\partial E_{ij}} + \frac{\partial w}{\partial I_2} \frac{\partial I_2}{\partial E_{ij}} + \frac{\partial w}{\partial I_3} \frac{\partial I_3}{\partial E_{ij}}\right] \tag{1.129}$$

where

$$\left.\begin{aligned} \frac{\partial I_1}{\partial E_{ij}} &= 2\delta_{ij} \\ \frac{\partial I_2}{\partial E_{ij}} &= 2(\delta_{ij}\delta_{rs} - \delta_{ir}\delta_{js})(2E_{rs} + \delta_{rs}) \\ \frac{\partial I_3}{\partial E_{ij}} &= 2 \frac{\partial X_i}{\partial x_m} \frac{\partial X_j}{\partial x_m} I_3 \end{aligned}\right\} \tag{1.130}$$

For an incompressible hyperelastic material, I_3 need not be considered. Then,

$$S_{ij} = \rho_0 \left[\frac{\partial w}{\partial I_1} \frac{\partial I_1}{\partial E_{ij}} + \frac{\partial w}{\partial I_2} \frac{\partial I_2}{\partial E_{ij}} \right] + h \frac{\partial X_i}{\partial x_m} \frac{\partial X_j}{\partial x_m} \tag{1.131}$$

By defining different deformation energy density functions, different hyperelastic material models could by defined. Some commonly used models are given below:

1. Neo Hooke model [3,29]

$$w = C_1(I_1 - 3) \tag{1.132}$$

2. Moony model [30–32]

$$W = C_1(I_1 - 3) + C_2(I_2 - 3) \tag{1.133}$$

where C_1 and C_2 are the material constants.

The deformation energy density functions of the above models are defined by the invariables of Green deformation tensor. Because $C_{ii} = \lambda_i^2$, λ_i is the principal stretch; the deformation energy density functions of the models are functions of even power of λ_i, so they belong to the Rivilin materials. For the Rivilin materials, the deformation energy density functions can be chosen as functions of higher-order power of I_1 and I_2. With an increase in the order, or the number of the items, the agreement of the constitutive equation with the behavior of real materials will be improved, but the parameters to be determined increase, and the computation becomes more complicated. It is found that I_3 is not included in the deformation energy density functions of the above models, so they are incompressible hyperelastic materials.

3. Ogden model [33,34]
Volume change in deformation is taken into account in this model. Its deformation energy density function is

$$w = \sum_{n=1}^{N} \frac{\mu_n}{\alpha_n} \left[J^{\frac{-\alpha_n}{3}} \left(\lambda_1^{\alpha_n} + \lambda_2^{\alpha_n} + \lambda_3^{\alpha_n} \right) - 3 \right] + 4.5K \left(J^{\frac{1}{3}} - 1 \right)^2 \tag{1.134}$$

where

μ_n and α_n are the material constants

K is the voluminal modulus

J is the ratio of volume change expressed as $J = \lambda_1 \lambda_2 \lambda_3$

Equation 1.134 should be applied in case the ratio of volume change is in the order of 0.01. If volume change is large, the following generalized compressible Ogden model could be used:

$$w = \sum_{n=1}^{N} \frac{\mu_n}{\alpha_n} \left[\lambda_1^{\alpha_n} + \lambda_2^{\alpha_n} + \lambda_3^{\alpha_n} - 3 \right] + \sum_{n=1}^{N} \frac{\mu_n}{\beta_n} (1 - J^{\beta_n}) \tag{1.135}$$

where μ_n, α_n, and β_n are the material constants. Usually $N = 2$ or $N = 3$ is appropriate.

1.5.2 Elastoplastic Constitutive Equation

1.5.2.1 Introduction

The plastic behavior of the metal at normal temperature depends on deformation history of the material, hence the plastic flow theory, that establishes the relationship between stress rate and strain rate, should be normally used.

In establishing the constitutive equation, first a small deformation problem is considered, and the relationship between Cauchy stress and small strain is established. Then the constitutive equation is extended to finite-deformation problem; here Cauchy stress and small strain should be substituted by corresponding appropriate stress rate and strain rate. The appropriate stress rate could be chosen as Jaumann rate of Cauchy stress, $\hat{\boldsymbol{\sigma}}$, and the objective strain rate could be chosen as the rate of deformation tensor, $\mathbf{d}$.

The elastoplastic deformation is decomposed into a recoverable elastic deformation and an unrecoverable plastic deformation. In small deformation, the strain increment $\mathrm{d}\boldsymbol{\varepsilon}$ is decomposed as follows:

$$\mathrm{d}\boldsymbol{\varepsilon} = \mathrm{d}\boldsymbol{\varepsilon}^{\mathrm{e}} + \alpha \mathrm{d}\boldsymbol{\varepsilon}^{\mathrm{p}}$$

Correspondingly, in finite deformation, the strain rate, $\mathbf{d}$, is decomposed as

$$\mathbf{d} = \mathbf{d}^{\mathrm{e}} + \alpha \mathbf{d}^{\mathrm{p}}$$

where

superscripts ''e'' and ''p'' mean the elastic and plastic components, respectively
α is the loading factor

In pure elastic deformation, including unloading, $\alpha = 0$; in elastoplastic deformation, $\alpha = 1$.

1.5.2.2 Yield Criterion

When a metal sample is deformed under uniaxial loading, if the deformation is small, the material is in elastic state, and the relation between stress and strain is linear. When the stress reaches the yield point, σ_{s}, the material yields and deforms plastically, and the relation between stress and strain becomes nonlinear.

In a deforming body, the stress distribution is generally not uniform. For a particle in the material, when the stress components meet a certain condition, the particle will yield. This condition is called yield criterion. The yield criterion can be written in the following general mathematical expression:

$$F = f(\sigma_{ij}) - \sigma_{\mathrm{s}} = 0 \tag{1.136}$$

where

$f(\sigma_{ij})$ is the function of the stress components
σ_{s} is the initial yield stress

The yield criterion may be geometrically represented by a surface in the stress space, called yield surface. If the stress, σ_{ij}, locates inside the surface, i.e., $F(\sigma_{ij}) < 0$, then the particle is in elastic state. If the stress, σ_{ij}, locates on the surface, i.e., $F(\sigma_{ij}) = 0$, then the particle yields and turns into the plastic state. But it is impossible for the stress, σ_{ij}, to get out the surface, i.e., $F(\sigma_{ij}) > 0$.

1.5.2.3 Flow Rule

1.5.2.3.1 Associated Flow Rule

For ordinary engineering materials, the flow stress is an increasing function of the plastic strain in plastic deformation; such material is called a stable material, which meets the condition $\Delta\sigma_{ij}\,\Delta\varepsilon_{ij} > 0$ during plastic deformation. Consequently, successive yield surface, or loading surface, $F(\sigma_{ij}, Y)$ is convex. Let the stress space coincide with the strain space; then the plastic strain increment must point in the outward normal direction of the yield surface $F(\sigma_{ij}, Y)$, i.e.,

$$\dot{\varepsilon}_{ij} = \dot{\lambda}\,\frac{\partial F}{\partial \sigma_{ij}} \tag{1.137}$$

where

$\partial F/\partial\sigma_{ij}$, the geometric meaning of the partial derivative, is the component of the unit outward normal vector of the yield surface F, in the stress space

$\dot{\lambda}$ is the scalar factor

Adopting the concept of plastic potential theory, F is taken as the plastic potential function. When the yield criterion is taken as the plastic potential function, associated flow rule can be obtained. Using a different yield function, different plastic stress–strain relationships can be derived from associated flow rule. If the plastic potential function is not chosen as the yield criterion, the resulting plastic stress–strain relationship is called nonassociated flow rule. For metals, associated flow rule is normally used.

1.5.2.3.2 Loading–Unloading Condition

Work hardening usually occurs in plastic deformation of metals at normal temperature, which causes an increase in successive yield stress or flow stress. Successive yield criterion can normally be written as

$$F = f(\sigma) - Y(\overline{\varepsilon}^{\mathrm{P}}) = 0$$

where Y is the flow stress, and is usually taken as a function of the accumulated plastic strain, $\overline{\varepsilon}^{\mathrm{P}}$. In small elastoplastic deformation, the loading–unloading condition of work hardening material is as follows.

Loading:

$$F = 0, \quad \mathrm{d}F = 0 \quad \text{and} \quad \frac{\partial F}{\partial \sigma_{ij}}\mathrm{d}\sigma_{ij} > 0$$

Unloading:

$$F = 0, \quad \mathrm{d}F < 0 \tag{1.138}$$

Neutral variation:

$$F = 0, \quad \mathrm{d}F = 0 \quad \text{and} \quad \frac{\partial F}{\partial \sigma_{ij}}\mathrm{d}\sigma_{ij} = 0$$

where, the geometric meaning of $(\partial F/\partial\sigma_{ij})\mathrm{d}\sigma_{ij}$ is the projection of stress increment, $\mathrm{d}\boldsymbol{\sigma}$, in the outward unit normal vector of the yield surface, $\partial F/\partial\boldsymbol{\sigma}$. In loading state, the value of the projection

is positive. During loading, $F=0$ and $\mathrm{d}F=0$ must be satisfied; they are called consistency condition. From the consistency condition, we obtain

$$\frac{\partial F}{\partial \sigma_{ij}}\mathrm{d}\sigma_{ij} - \mathrm{d}Y = 0$$

Since $\overline{\sigma}=Y$ and $\mathrm{d}\overline{\sigma}=\mathrm{d}Y$ during loading, the above equation can be written as

$$\frac{\partial F}{\partial \sigma_{ij}}\mathrm{d}\sigma_{ij} - \mathrm{d}\overline{\sigma} = 0$$

1.5.2.4 Hardening Law

1.5.2.4.1 Two Kinds of Hardening Assumptions

For hardened materials, it is assumed that the successive yield behavior still obeys the initial yield criterion, but the initial yield stress must be replaced by flow stress.

The change in successive yield surface, and yield locus, which is the intersection of the yield surface with a plane in the stress space, is very complicated. For simplicity, two kinds of assumptions are commonly adopted. One of them is the isotropic hardening assumption. Its key points are (1) the material remains isotropic after hardening; (2) the center and the shape of the yield locus do not change after hardening, but its size grows continuously during deformation. The other is the kinematic hardening assumption. Its key point is that the size and shape of the yield locus is fixed after hardening, and the yield locus only moves rigidly in the stress space. Sometimes both assumptions are combined in application.

1.5.2.4.2 Equivalent Stress–Equivalent Strain Relation

Flow stress is the function of accumulated plastic strain or plastic work; their relationship can be determined by the single curve assumption. It is assumed that in the equivalent stress–equivalent strain relationship in general the stress state is identical with the true stress–true strain relationship in uniaxial stress state.

The commonly used formulations describing the relationship between equivalent stress and equivalent strain are given below. These formulations only describe the equivalent stress and equivalent strain relationship in plastic state; the consistency between elastic and plastic stress–strain relationships can be realized by the compatibility of initial yield stress $\overline{\sigma}_{s_0}$.

1. Ideal plasticity

$$\overline{\sigma} = \sigma_s$$

   where, work hardening is neglected.
2. Linear hardening

$$\overline{\sigma} = \sigma_s + K\overline{\varepsilon}$$

   where K is the tangent modulus.
3. Power law

$$\overline{\sigma} = K\overline{\varepsilon}^n$$

   where
   K is the strength factor
   n the hardening exponent.

4. Power law with initial strain

$$\overline{\sigma} = K(\overline{\varepsilon}_0 + \overline{\varepsilon})^n$$

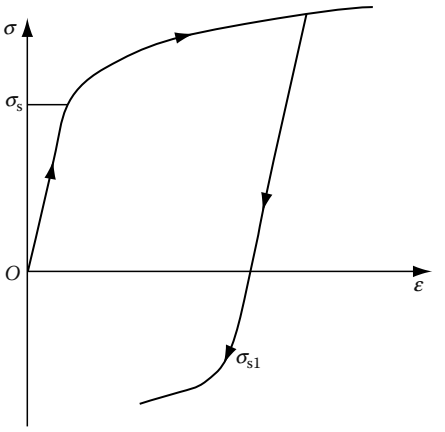

FIGURE 1.9 True stress–true strain curve.

1.5.2.4.3 Bauschinger Effect

For metals, if loading direction is reversed after plastic deformation, the yield stress in reverse loading direction is lower than the initial yield stress, as shown in Figure 1.9. This phenomenon is called Bauschinger effect and can be described by the kinematic hardening assumption.

1.5.2.5 Commonly Used Plastic Constitutive Equations

1.5.2.5.1 J_2 Flow Rule

Supposing the material is plastically isotropic, as the yield criterion is an appropriate physical law, it can be expressed as the function of stress invariants. Since hydrostatic pressure does not affect yielding, the yield criterion is related only with the deviatoric stress. Consequently, the yield condition can be written as

$$F(J_2', J_3') = 0$$

where J_2' and J_3' are the second and third invariants of the deviatoric stress, σ_{ij}'. It should be noted that $J_1' = 0$.

For the isotropic hardening material, the von Mises yield criterion can be written as

$$F = \sqrt{\frac{3}{2}\sigma_{ij}'\sigma_{ij}'} - Y = \sqrt{3J_2'} - Y = 0 \tag{1.139}$$

Since the yield criterion is the function of the second invariant of deviatoric stress, J_2', the associated flow rule derived by it is called the J_2 flow rule.

Von-Mises yield criterion can be represented geometrically by a cylinder in the principal stress space; the axis of the cylinder is along the isoclinal direction, and its radius is $\sqrt{2/3}\ Y$, as shown in Figure 1.10. In principal stress space, the plane passing through the origin and normal to the isoclinal direction is called π plane. The Mises yield locus in π plane is a circle.

Substituting the Mises yield criterion into the associated flow rule, we get

$$\dot{\varepsilon}_{ij}^{\mathrm{p}} = \dot{\lambda}\sigma_{ij}' \tag{1.140}$$

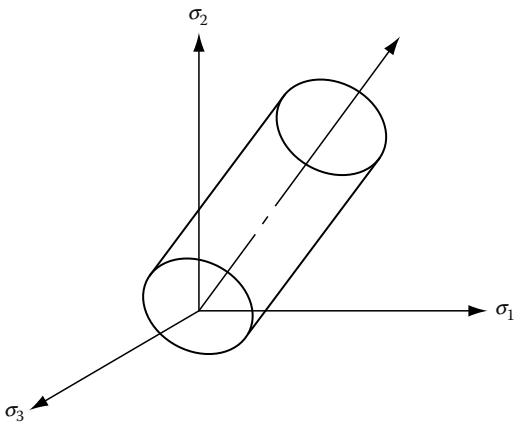

FIGURE 1.10 Mises yielding surface in the principal stress space.

If both sides of the above equation are multiplied by themselves and then summed, $\dot{\lambda}$ is obtained

$$\dot{\lambda} = \frac{3}{2}\frac{\dot{\overline{\varepsilon}}^{\mathrm{p}}}{\overline{\sigma}}$$

where $\overline{\sigma}$ and $\dot{\overline{\varepsilon}}$ are the equivalent stress and equivalent strain rates, respectively, which are defined as

$$\overline{\sigma}^2 = \frac{3}{2}\sigma'_{ij}\sigma'_{ij}$$

$$\dot{\overline{\varepsilon}}^2 = \frac{2}{3}\dot{\varepsilon}_{ij}\dot{\varepsilon}_{ij}$$

Substituting the above equations into Equation 1.140, the Saint-Venant flow equation is obtained.

$$\dot{\varepsilon}^{\mathrm{p}}_{ij} = \frac{3}{2}\frac{\dot{\overline{\varepsilon}}^{\mathrm{p}}}{\overline{\sigma}}\sigma'_{ij}$$

Its incremental form is

$$\mathrm{d}\varepsilon^{\mathrm{p}}_{ij} = \frac{3\mathrm{d}\overline{\varepsilon}^{\mathrm{p}}}{2\overline{\sigma}}\sigma'_{ij} \tag{1.141}$$

1.5.2.5.2 Kinematic Hardening Rule

Supposing the initial yield criterion is

$$F = \sqrt{3J'_2} - \sigma_{\mathrm{s}_0} = 0$$

During plastic deformation, σ_{s_0} in the above equation remains constant. This model is called the J_2 kinematic hardening model. Supposing the center of the yield surface moves to θ_{ij}, the successive yield criterion can be written as

$$F = \sqrt{\frac{3}{2}(\sigma'_{ij} - \theta'_{ij})(\sigma'_{ij} - \theta'_{ij})} - \sigma_{\mathrm{s}_0} = 0 \tag{1.142}$$

where θ'_{ij} is the deviator of θ_{ij}; θ_{ij} is called backing stress.

$$\frac{\partial F}{\partial \sigma_{ij}} = \frac{3(\sigma'_{ij} - \theta'_{ij})}{2\sigma_{s_0}}$$

The equivalent stress is defined as

$$\overline{\sigma}'^2 = \frac{3}{2}(\sigma'_{ij} - \theta'_{ij})(\sigma'_{ij} - \theta'_{ij})$$

When $(\sigma'_{ij} - \theta'_{ij})\hat{\sigma}_{ij} > 0$ and $\overline{\sigma}' = \sigma_{s_0}$, $\alpha = 1$; when $(\sigma'_{ij} - \theta'_{ij})\hat{\sigma}_{ij} < 0$ or $\overline{\sigma}' < \sigma_{s_0}$, $\alpha = 0$.

The movement of the center of the yield surface, θ, can be determined by Ziegler rule. It is assumed that during plastic deformation, θ moves along the direction of vector $\sigma - \theta$; then

$$\hat{\theta}_{ij} = \hat{\mu}(\sigma_{ij} - \theta_{ij})$$

where $\hat{\theta}_{ij}$ is the Jaumann rate of θ_{ij}.

From the consistency condition, we obtain

$$\hat{\mu} = \frac{3(\sigma'_{ij} - \theta'_{ij})}{2\sigma^2_{s_0}}\hat{\sigma}_{ij}$$

It is found that if the kinematic hardening rule with Jaumann rate is used in analyzing the simple shear deformation, after shear strain exceeds 1, shear stress will oscillate, which is unreasonable. To prevent such a problem, it is suggested that Jaumann rate be substituted by Green–Naghdi rate in the constitutive equation, i.e., the rotational speed $\boldsymbol{\omega}$ be substituted by $\mathbf{W}_{\mathrm{R}} = \dot{\mathbf{R}} \cdot \mathbf{R}^{\mathrm{T}}$.

1.5.2.5.3 Orthotropic Material

Hill proposed the yield criterion for orthotropic materials in 1948:

$$F(\sigma_{22} - \sigma_{33}) + G(\sigma_{33} - \sigma_{11})^2 + H(\sigma_{11} - \sigma_{22})^2 + 2L\sigma^2_{23} + 2M\sigma^2_{31} + 2N\sigma^2_{12} = 1 \qquad (1.143)$$

where

F, G, H, L, M, and N are the anisotropic parameters

x_1, x_2, and x_3 are the material anisotropic principal axes

Let $\overline{\sigma}$ denote the equivalent stress and Y the flow stress:

$$\overline{\sigma} = \sqrt{\frac{3}{2}\frac{F(\sigma_{22} - \sigma_{33})^2 + G(\sigma_{33} - \sigma_{11})^2 + H(\sigma_{11} - \sigma_{22})^2 + 2L\sigma^2_{23} + 2M\sigma^2_{31} + 2N\sigma^2_{12}}{F + G + H}}$$

$$Y = \sqrt{\frac{3}{2(F + G + H)}}$$

Then Equation 1.143 can be rewritten in the following form:

$$\overline{F} = \overline{\sigma} - Y = 0$$

According to the associated flow law,

$$\mathrm{d}\varepsilon_{ij}^{\mathrm{p}} = \mathrm{d}\lambda \frac{\partial \overline{F}}{\partial \sigma_{ij}} = \mathrm{d}\lambda \frac{Y^2}{\overline{\sigma}} A_{ij}$$

where

$$A_{11} = G(\sigma_{11} - \sigma_{33}) + H(\sigma_{11} - \sigma_{22})$$

$$A_{22} = F(\sigma_{22} - \sigma_{33}) + H(\sigma_{22} - \sigma_{11})$$

$$A_{33} = G(\sigma_{33} - \sigma_{11}) + F(\sigma_{33} - \sigma_{22})$$

$$A_{12} = A_{21} + N\sigma_{12}$$

$$A_{23} = A_{32} = L\sigma_{23}$$

$$A_{31} = A_{13} = M\sigma_{31}$$

$$\mathrm{d}\lambda = \mathrm{d}\overline{\varepsilon}^{\mathrm{p}} = \frac{YC_{mnpq}^{\mathrm{e}} A_{mn} \mathrm{d}\varepsilon_{pq}}{E_t + Y^2 C_{mnpq}^{\mathrm{e}} A_{mn} A_{pq}}$$

For a plane stress problem, e.g., the sheet metal forming problem, the yield criterion is simplified as

$$\overline{F} = \frac{3}{2(F+G+H)} \left[(G+H)\sigma_{11}^2 + (F+H)\sigma_{22}^2 - 2H\sigma_{11}\sigma_{22} + 2N\sigma_{12}^2 \right] - Y^2 = 0$$

The coefficients in the above equation can be determined by the strain ratio in transverse and thickness directions during simple tension, $r = \varepsilon_{\mathrm{t}}/\varepsilon_{\mathrm{z}}$. Let r_0, r_{45}, and r_{90} denote the strain ratio along the direction 0°, 45°, and 90° from the rolling direction, respectively, σ_{s_1}, $\sigma_{\mathrm{s}_{45}}$, and σ_{s_2} the yield stresses in simple tension along and above directions respectively; then

$$G = \frac{1}{(1+r_0)\sigma_{\mathrm{s}_1}^2}$$

$$F = \frac{1}{(1+r_{90})\sigma_{\mathrm{s}_2}^2}$$

$$H = \frac{r_0}{(1+r_0)\sigma_{\mathrm{s}_1}^2} = \frac{r_{90}}{(1+r_{90})\sigma_{\mathrm{s}_2}^2}$$

$$N = (G+H)\left(\frac{1}{2} + r_{45}\right)$$

Supposing $r = r_0 = r_{45} = r_{90}$, (i.e., the sheet is anisotropic along the thickness direction, but isotropic in the horizontal plane where x, y directions coincide with the principal stress directions), then, the yield criterion can be further simplified as

$$\overline{F} = \frac{3}{2(2+r)} \left[(1+r)(\sigma_1^2 + \sigma_2^2) - 2r\sigma_1\sigma_2 \right] - Y^2 = 0$$

In this condition, the following relationship among the anisotropic parameters exists. Let $\sigma_{s_1} = \sigma_{s_2} = \sigma_s$, then

$$F = G = \frac{1}{(1+r)\sigma_s^2}$$
$$H = rF$$
$$N = (1+2r)F$$
$$L = M = \frac{(5+r)}{2}F$$
$$Y^2 = \frac{3(1+r)\sigma_s^2}{2(2+r)}$$

when r is more than unity, i.e., $r > 1$, this yield criterion cannot describe the abnormal phenomenon of the ratio of σ_b and σ_u less than unity, i.e., $\sigma_b/\sigma_u < 1$, where σ_b means the yield stress in biaxial tension, and σ_u the yield stress in simple tension. Therefore, Hill, Bassani, et al. proposed nonquadratic yield criteria. However, the original form of the orthotropic yield criterion is more convenient and commonly used.

1.5.2.5.4 Compressible Material

Some materials, such as metal powder, have volume change during plastic deformation; besides deviatoric and hydrostatic stress also affect their yielding. The yield criterion can be written as

$$F = AJ_2' + BJ_1^2 - CY^2 = 0 \tag{1.144}$$

where

J_2' is the second invariant of the deviatoric stress tensor
J_1 is the first invariant of the stress tensor
Y is the flow stress of matrix material
A, B, and C are the function of void volume fraction, $f = V_{cavity}/(V_{matrix} + V_{cavity})$, or the mass density, ρ

They should be determined by experiments.

From the associated flow rule, we obtain

$$\dot{\varepsilon}_{ij}^{p} = \frac{3\dot{\bar{\varepsilon}}}{2\bar{\sigma}}\left(A\sigma_{ij}' + 2BJ_1\delta_{ij}\right)$$
$$\dot{\varepsilon}_{kk} = \frac{3\dot{\bar{\varepsilon}}}{\bar{\sigma}}BJ_1$$

The equivalent stress and equivalent strain are defined respectively as

$$\bar{\sigma}^2 = 3(AJ_2' + BJ_1^2)$$
$$\dot{\bar{\varepsilon}}^2 = \frac{2}{3}\left[\frac{1}{A}\dot{\varepsilon}_{ij}'\dot{\varepsilon}_{ij}' + \frac{1}{18B}(\dot{\varepsilon}_{kk})^2\right]$$

If the material compressibility is small enough, then B approaches zero, i.e., $B \to 0$. If $A \to 1$ and $C \to 1/3$ are also assumed, then the yield criterion, the equivalent stress, and the equivalent strain of voided material coincide with those defined by Mises criterion. For A and B, the relation $A + 3B = 1$ should be satisfied.

1.5.2.6 Elastoplastic Constitutive Equation

The formulation of elastic constitutive equation and plastic flow rule were presented here separately. They are now combined to get the elastoplastic constitutive equation. First, the elastoplastic constitutive equation in small deformation is derived. If the yield criterion is written in such a form, in which the yield stress, Y, is in the first power, then in the associated flow rule $\mathrm{d}\lambda = \mathrm{d}\overline{\varepsilon}^{\mathrm{p}}$; i.e., the associated flow rule can be expressed as $\mathrm{d}\varepsilon_{kl}^{\mathrm{p}} = \mathrm{d}\overline{\varepsilon}^{\mathrm{p}}(\partial F/\partial\sigma_{kl})$. Substituting this equation into Equation 1.117, we get

$$\mathrm{d}\sigma_{ij} = C_{ijkl}^{\mathrm{e}}(\mathrm{d}\varepsilon_{kl} - \mathrm{d}\varepsilon_{kl}^{\mathrm{p}}) = C_{ijkl}^{\mathrm{e}}\left(\mathrm{d}\varepsilon_{kl} - \mathrm{d}\overline{\varepsilon}^{\mathrm{p}}\frac{\partial F}{\partial\sigma_{kl}}\right)$$

If both sides of the above equation are multiplied by $\partial F/\partial\sigma_{ij}$ and summed up, we get

$$\frac{\partial F}{\partial\sigma_{ij}}\mathrm{d}\sigma_{ij} = \frac{\partial F}{\partial\sigma_{ij}}C_{ijkl}^{\mathrm{e}}\left(\mathrm{d}\varepsilon_{kl} - \mathrm{d}\overline{\varepsilon}^{\mathrm{p}}\frac{\partial F}{\partial\sigma_{kl}}\right)$$

Applying the consistency condition, $(\partial F/\partial\sigma_{ij})\,\mathrm{d}\sigma_{ij} = \mathrm{d}\overline{\sigma}$, and supposing $H = \mathrm{d}\overline{\sigma}/\mathrm{d}\overline{\varepsilon}^{\mathrm{p}}$, the above equation can be written as

$$H\mathrm{d}\overline{\varepsilon}^{\mathrm{p}} = \frac{\partial F}{\partial\sigma_{ij}}C_{ijkl}^{\mathrm{e}}\left(\mathrm{d}\varepsilon_{kl} - \mathrm{d}\overline{\varepsilon}^{\mathrm{p}}\frac{\partial F}{\partial\sigma_{kl}}\right)$$

$\mathrm{d}\overline{\varepsilon}^{\mathrm{p}}$ can be solved from the above equation:

$$\mathrm{d}\overline{\varepsilon}^{\mathrm{p}} = \frac{\frac{\partial F}{\partial\sigma_{ij}}C_{ijkl}^{\mathrm{e}}\mathrm{d}\varepsilon_{kl}}{H + \frac{\partial F}{\partial\sigma_{ij}}C_{ijkl}^{\mathrm{e}}\frac{\partial F}{\partial\sigma_{kl}}}$$

Then, the general form of the elastoplastic constitutive equation referring to the stress increment in small deformation condition is obtained:

$$\begin{aligned}\mathrm{d}\sigma_{ij} &= \left[C_{ijkl}^{\mathrm{e}} - \alpha\frac{C_{ijmn}^{\mathrm{e}}\frac{\partial F}{\partial\sigma_{mn}}\frac{\partial F}{\partial\sigma_{rs}}C_{rskl}^{\mathrm{e}}}{H + \frac{\partial F}{\partial\sigma_{mn}}C_{mnrs}^{\mathrm{e}}\frac{\partial F}{\partial\sigma_{rs}}}\right]\mathrm{d}\varepsilon_{kl} \\ &= \left(C_{ijkl}^{\mathrm{e}} - \alpha C_{ijkl}^{\mathrm{p}}\right)\mathrm{d}\varepsilon_{kl} = C_{ijkl}^{\mathrm{ep}}\mathrm{d}\varepsilon_{kl}\end{aligned} \tag{1.145}$$

where α is the loading factor. For example, if Mises yield criterion is substituted into the above equation, the elastoplastic constitutive equation of J_2 flow rule in small deformation condition can be obtained.

$$\mathrm{d}\sigma_{ij} = \left(C_{ijkl}^{\mathrm{e}} - \frac{2G\alpha}{g}\sigma'_{ij}\sigma'_{kl}\right)\mathrm{d}\varepsilon_{kl} = C_{ijkl}^{\mathrm{ep}}\mathrm{d}\varepsilon_{kl}$$

where, G is the shear modulus, $g = 2\overline{\sigma}^2[1 + h/(2G)]/3$, and $h = 2H/3$. Let E denote the slope of the stress–strain curve of simple tension, assuming that the material is incompressible; then

$$\frac{1}{H} = \mathrm{d}\varepsilon^{\mathrm{p}}/\mathrm{d}\sigma = (\mathrm{d}\varepsilon - \mathrm{d}\varepsilon^{\mathrm{e}})/\mathrm{d}\sigma = 1/E_{\mathrm{t}} - 1/E$$

In finite strain, $d\sigma_{ij}$ and $d\varepsilon_{ij}^{p}$ in the loading–unloading criterion, flow rule and the elastoplastic constitutive equation should be substituted by $\hat{\sigma}_{ij}$ and d_{ij}^{p}, respectively.

1.5.2.7 Thermal Elastoplastic Constitutive Equation

1.5.2.7.1 Thermal Elastic Constitutive Equation

In the elastic zone, the strain, expressed by a vector, is decomposed as follows:

$$d\boldsymbol{\varepsilon} = d\boldsymbol{\varepsilon}^{e} + d\boldsymbol{\varepsilon}^{T} = d\boldsymbol{\varepsilon}^{e} + \boldsymbol{\alpha} dT \tag{1.146}$$

where

$d\boldsymbol{\varepsilon}^{T}$ is the thermal strain increment caused by thermal expansion; only the normal strain components are nonzero

$\boldsymbol{\alpha}$ is the vector of the thermal expansion coefficients, $\boldsymbol{\alpha} = \alpha\ [1\ 1\ 1\ 0\ 0\ 0]^{T}$

From the Hooke's law

$$\boldsymbol{\varepsilon}^{e} = (\mathbf{C}^{e})^{-1}\boldsymbol{\sigma}$$

Since the elastic matrix, $\mathbf{C}^{e}$, depends on the temperature, T, differentiation of the above equation leads to

$$d\boldsymbol{\varepsilon}^{e} = \frac{d(\mathbf{C}^{e})^{-1}}{dT}\boldsymbol{\sigma} dT + (\mathbf{C}^{e})^{-1} d\boldsymbol{\sigma}$$

Substituting the above equation into Equation 1.146, $d\boldsymbol{\sigma}$ can be solved:

$$d\boldsymbol{\sigma} = \mathbf{C}^{e}\left[d\boldsymbol{\varepsilon} - (\boldsymbol{\alpha} + \frac{d(\mathbf{C}^{e})^{-1}}{dT}\boldsymbol{\sigma})dT\right]$$

If the variation of the elastic properties with changing temperature can be neglected, we obtain

$$d\boldsymbol{\sigma} = \mathbf{C}^{e}(d\boldsymbol{\varepsilon} - d\boldsymbol{\varepsilon}^{T})$$

1.5.2.7.2 Thermal Elastoplastic Constitutive Equation

In the plastic zone, since the flow stress, Y, depends on the temperature, T, the successive Mises yield criterion can be written as

$$F = \overline{\sigma} - Y\left(\int d\overline{\varepsilon}^{p}, T\right) = 0$$

The differentiation of the above equation is

$$\frac{\partial F}{\partial \boldsymbol{\sigma}} d\boldsymbol{\sigma} = H d\overline{\varepsilon}^{p} + \frac{\partial Y}{\partial T} dT$$

where

$$H = \frac{\mathrm{d}Y}{\mathrm{d}\overline{\varepsilon}^{\mathrm{p}}}$$

$$\frac{\partial F}{\partial \boldsymbol{\sigma}} = \left[\frac{\partial F}{\partial \sigma_{11}} \; \frac{\partial F}{\partial \sigma_{22}} \; \frac{\partial F}{\partial \sigma_{33}} \; \frac{\partial F}{\partial \sigma_{12}} \; \frac{\partial F}{\partial \sigma_{23}} \; \frac{\partial F}{\partial \sigma_{33}}\right]^{\mathrm{T}}$$

In the plastic zone

$$\mathrm{d}\boldsymbol{\varepsilon} = \mathrm{d}\boldsymbol{\varepsilon}^{\mathrm{e}} + \mathrm{d}\boldsymbol{\varepsilon}^{\mathrm{p}} + \mathrm{d}\boldsymbol{\varepsilon}^{\mathrm{T}}$$

Substituting Equation 1.146 and the flow rule into the above equation, $\mathrm{d}\boldsymbol{\sigma}$ can be solved.

$$\mathrm{d}\boldsymbol{\sigma} = \mathbf{C}^{\mathrm{e}}\left[\mathrm{d}\boldsymbol{\varepsilon} - \frac{\partial F}{\partial \boldsymbol{\sigma}}\mathrm{d}\overline{\varepsilon}^{\mathrm{p}} - \left(\boldsymbol{\alpha} + \frac{\mathrm{d}(\mathbf{C}^{\mathrm{e}})^{-1}}{\mathrm{d}T}\boldsymbol{\sigma}\right)\mathrm{d}T\right]$$

If both sides of the above equation are multiplied by $\partial F/\partial \boldsymbol{\sigma}$, and then summed up, $\mathrm{d}\overline{\varepsilon}^{\mathrm{p}}$ can be solved.

$$\mathrm{d}\overline{\varepsilon}^{\mathrm{p}} = \frac{\left(\frac{\partial F}{\partial \boldsymbol{\sigma}}\right)^{\mathrm{T}}\mathbf{C}^{\mathrm{e}}\mathrm{d}\boldsymbol{\varepsilon} - \left(\frac{\partial F}{\partial \boldsymbol{\sigma}}\right)^{\mathrm{T}}\mathbf{C}^{\mathrm{e}}\left(\boldsymbol{\alpha} + \frac{\mathrm{d}(\mathbf{C}^{\mathrm{e}})^{-1}}{\mathrm{d}T}\boldsymbol{\sigma}\right)\mathrm{d}T - \frac{\partial Y}{\partial T}\mathrm{d}T}{H + \left(\frac{\partial F}{\partial \boldsymbol{\sigma}}\right)^{\mathrm{T}}\mathbf{C}^{\mathrm{e}}\frac{\partial F}{\partial \boldsymbol{\sigma}}}$$

Then, the incremental stress–strain relationship in the plastic zone is obtained.

$$\mathrm{d}\boldsymbol{\sigma} = \mathbf{C}^{\mathrm{ep}}\left[\mathrm{d}\boldsymbol{\varepsilon} - \left(\boldsymbol{\alpha} + \frac{\mathrm{d}(\mathbf{C}^{\mathrm{e}})^{-1}}{\mathrm{d}T}\boldsymbol{\sigma}\right)\mathrm{d}T\right] + \mathrm{d}\overline{\boldsymbol{\sigma}}^{\mathrm{T}} \approx \mathbf{C}^{\mathrm{ep}}(\mathrm{d}\boldsymbol{\varepsilon} - \mathrm{d}\boldsymbol{\varepsilon}^{\mathrm{T}}) + \mathrm{d}\overline{\boldsymbol{\sigma}}^{\mathrm{T}} \tag{1.147}$$

where $\mathrm{d}\overline{\boldsymbol{\sigma}}^{\mathrm{T}}$ denotes the additional stress arising from the effect of temperature on the plastic modulus:

$$\mathrm{d}\overline{\boldsymbol{\sigma}}^{\mathrm{T}} = \frac{\mathbf{C}^{\mathrm{e}}\frac{\partial F}{\partial \boldsymbol{\sigma}}\frac{\partial Y}{\partial T}\mathrm{d}T}{H + \left(\frac{\partial F}{\partial \boldsymbol{\sigma}}\right)^{\mathrm{T}}\mathbf{C}^{\mathrm{e}}\frac{\partial F}{\partial \boldsymbol{\sigma}}}$$

1.5.2.7.3 Phase Transformation

When multiple phases exist in the material, each material parameter, such as the Young's modulus, E, the flow stress, Y, etc., should be taken as weighted averaging values:

$$A = \sum_{i=1}^{n} m_i A_i$$

where

A is the parameter value after weighted averaging
n is the number of phases
m_i is the percentage of phase i at the moment
A_i is the value of the parameter for phase i

Phase transformation causes a change in the specific volume of the material; such an effect is similar to thermal expansion and may be computed by an equivalent thermal expansion coefficient. Let β_j denote the thermal expansion coefficient corresponding to the specific volume change caused by transformation of phase j; then

$$\beta = \sum_{j=1}^{n} m_j \beta_j$$

where

β is the average thermal expansion coefficient; it is the function of temperature, T
n is the number of phases
m_j is the increment of phase j in the computation step

Then the strain increment is obtained:

$$\Delta \boldsymbol{\varepsilon}_{tr}^{\mathrm{e}} = \beta [1\ 1\ 1\ 0\ 0\ 0]^{\mathrm{T}} \Delta T$$

1.5.2.7.4 Loading–Unloading Condition

Considering the effects of temperature on the flow stress and the equivalent stress–equivalent strain curve, the loading–unloading condition is modified as follows:

$$\left.\begin{aligned} \text{Loading:}\quad & \left(\frac{\partial F}{\partial \boldsymbol{\sigma}}\right)^{\mathrm{T}} \mathrm{d}\boldsymbol{\sigma} + \frac{\partial F}{\partial T}\mathrm{d}T > 0 \\ \text{Unloading:}\quad & \left(\frac{\partial F}{\partial \boldsymbol{\sigma}}\right)^{\mathrm{T}} \mathrm{d}\boldsymbol{\sigma} + \frac{\partial F}{\partial T}\mathrm{d}T < 0 \\ \text{Neutral variation:}\quad & \left(\frac{\partial F}{\partial \boldsymbol{\sigma}}\right)^{\mathrm{T}} \mathrm{d}\boldsymbol{\sigma} + \frac{\partial F}{\partial T}\mathrm{d}T = 0 \end{aligned}\right\} \tag{1.148}$$

1.5.3 Viscoplastic Constitutive Equation

For materials deforming under impact loading and at high temperature, the yield stress and plastic modulus increase with an increase in the strain rate, as shown in Figure 1.11. Such behavior is called viscosity. The permanent deformation of viscoplastic material depends on time. For viscoplastic material, the strain rate can be decomposed into the elastic part and viscoplastic part. Here only its viscoplastic part, is consider denoted by superscript vp. A description of the elastic part can be found in the previous section. The viscoelastic response of the material is neglected.

1.5.3.1 One-Dimensional Viscoplastic Model

The mechanical model of viscoplastic material can be expressed by the combination of an elastic element, a plastic element, and a viscous element, as shown in Figure 1.12. The superscripts ''e,'' ''p,'' and ''vp'' in the figure mean elasticity, plasticity, and viscoplasticity, respectively. This kind of model takes into account viscosity only in the plastic part, not in elastic part. It is named elastic/viscoplastic model.

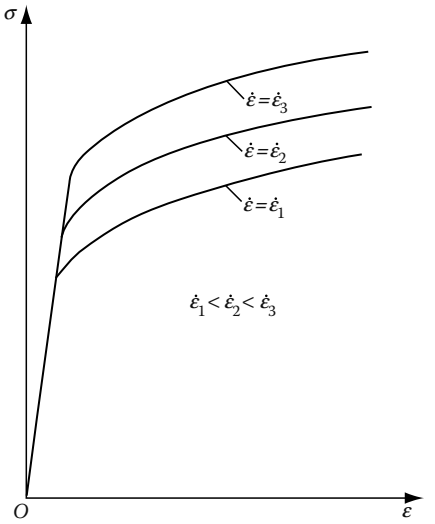

FIGURE 1.11 Stress–strain curve of viscoplastic material.

The constitutive relation of the elastic element is $\sigma = E\dot{\varepsilon}$. Let Y denote the static yield stress of the plastic element. The plastic element does not deform when $\sigma < Y$, and the stress applied to the plastic element keeps Y constant when $\sigma > Y$. The constitutive relation of the viscous element is $\sigma^{\mathrm{vp}} = \mu\dot{\varepsilon}^{\mathrm{vp}}$; here μ is the viscosity coefficient.

The total stress and strain rates meet the following relation:

$$\sigma = \sigma^{\mathrm{p}} + \sigma^{\mathrm{vp}}$$

$$\dot{\varepsilon} = \dot{\varepsilon}^{\mathrm{e}} + \dot{\varepsilon}^{\mathrm{vp}}$$

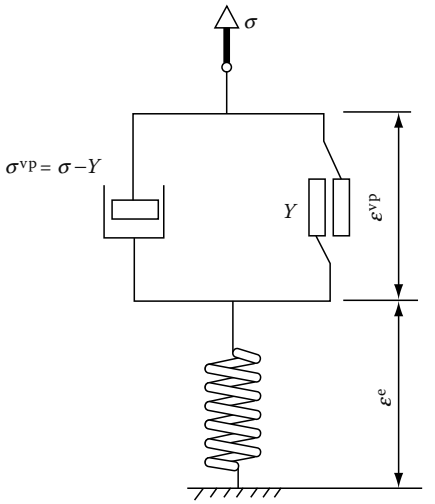

FIGURE 1.12 One-dimensional elastic/viscoplastic model.

Then the constitutive equation of elastic/viscoplastic material is

$$\left.\begin{aligned} \dot{\varepsilon} &= \frac{1}{E}\dot{\sigma} \quad \text{if } \sigma < \mathrm{Y} \\ \dot{\varepsilon} &= \frac{1}{E}\dot{\sigma} + \frac{1}{\mu}(\sigma - Y) \quad \text{if } \sigma > Y \end{aligned}\right\}$$

The stress exerted to the viscous element is $\sigma^{\mathrm{vp}} = \sigma - Y$, which is called overstress. If overstress exists, then $\dot{\varepsilon}$ cannot be zero, and the strain ε will increase with time.

1.5.3.2 Viscoplastic Constitutive Equation for General Stress State

Perzyna proposed the viscoplastic constitutive equation for general stress state by associated flow law of plastic potential theory.

$$\dot{\varepsilon}_{ij}^{\mathrm{vp}} = \gamma\langle\phi(F)\rangle\frac{\partial F}{\partial\sigma_{ij}} \tag{1.149}$$

where

γ is the viscous coefficient of the material
F is the static yield function

The meaning of the symbol $\langle\,\rangle$ is

$$\left.\begin{aligned} \langle\phi(F)\rangle &= 0 \quad \text{if } F < 0 \\ \langle\phi(F)\rangle &= \phi(F) \quad \text{if } F > 0 \end{aligned}\right\}$$

$\phi(F)$ is a function of overstress; it should be determined by experiment. For example, $\varphi(F) = (F/Y)^n$ can be adopted. If Mises yield criterion is adopted as F in the equation, we can finally obtain

$$\dot{\varepsilon}_{\mathrm{ij}}^{\mathrm{vp}} = \frac{3\dot{\overline{\varepsilon}}^{\mathrm{vp}}}{2\overline{\sigma}}\sigma'_{ij}$$

1.5.3.3 Commonly Used Viscoplastic Models

The flow stress of viscoplastic material is the function of strain, strain rate, and temperature, and the following expressions of equivalent stress are commonly used in engineering computations.

Backofen model [35–37]

$$\overline{\sigma} = c\dot{\overline{\varepsilon}}^{m}$$

where c and m are material constants.

Rosserd model [38–40]

$$\overline{\sigma} = k\overline{\varepsilon}^{m}\dot{\overline{\varepsilon}}^{n}$$

where k, m, and n are material constants. This model takes into account the effect of both strain and strain rate on flow stress.

The overstress model [41–43]

$$\overline{\sigma} = Y(\overline{\varepsilon})\left[1 + \left(\frac{\dot{\overline{\varepsilon}}^{\mathrm{vp}}}{r}\right)^{n}\right]$$

where
$Y(\overline{\varepsilon})$ is the static yield stress
n and r are the material constants

Power-exponent model [44,45]

$$\overline{\sigma} = g\left(\frac{\dot{\overline{\varepsilon}}^{\mathrm{vp}}}{\dot{a}}\right)^{m}$$

where
g is the reference stress
$\dot{a}$ is the reference strain rate
m is the material constant

1.5.3.4 Creep

If the material is loaded for a long time, especially at elevated temperature, then even the stress does not reach the yield stress, and it will deform permanently with time. If the stress is originated from the elastic deformation of the material, e.g., the prestress or residual stress, the stress will relax with time. This phenomenon is called creep. Creep is similar to viscoplasticity, and they differ in whether there exits the yield point and the time scale. A typical uniaxial creep curve is shown in Figure 1.13.

The duration of the initial creep and the third stage creep are short. Therefore, attention is usually concentrated on the second stage creep.

When analyzing creep problems, viscosity must be considered in both elastic and plastic constitutive responses. Such a constitutive model is called a viscoelastoplastic model.

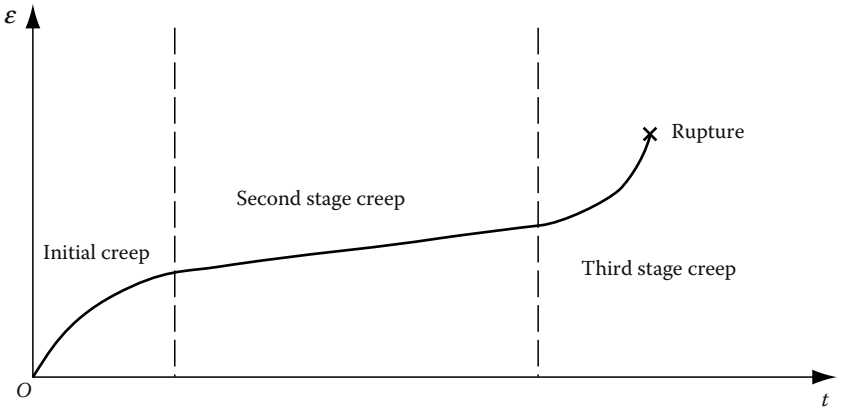

FIGURE 1.13 A typical one-dimensional creep curve.

The strain increment is decomposed as follows:

$$\Delta\boldsymbol{\varepsilon} = \Delta\boldsymbol{\varepsilon}^{\mathrm{e}} + \Delta\boldsymbol{\varepsilon}^{\mathrm{p}} + \Delta\boldsymbol{\varepsilon}^{\mathrm{T}} + \Delta\boldsymbol{\varepsilon}^{\mathrm{c}} \tag{1.150}$$

where the superscripts "e," "p," "T," and "c" denote the elastic, plastic, thermal, and creep strain, respectively.

Creep strain $\Delta\boldsymbol{\varepsilon}^{\mathrm{c}}$ can be expressed by creep strain rate $\dot{\varepsilon}^{\mathrm{c}}$. In the ith computation step

$$\Delta\boldsymbol{\varepsilon}_i^{\mathrm{c}} = \dot{\boldsymbol{\varepsilon}}_i^{\mathrm{c}}\Delta t_i(1-\theta) + \theta\dot{\boldsymbol{\varepsilon}}_{i+1}^{\mathrm{c}}\Delta t_i$$

where
Δt_i is the time step size of step i
$\dot{\boldsymbol{\varepsilon}}_i^{\mathrm{c}}$ and $\dot{\boldsymbol{\varepsilon}}_{i+1}^{\mathrm{c}}$ are the creep rate at time i and time $i+1$, respectively
θ is the parameter of finite difference, $0 \le \theta \le 1$

Usually $\theta = 1/2 \sim 2/3$ is adopted.

Suppose $\overline{\dot{\varepsilon}}^{\mathrm{c}}$ is the function of $\overline{\sigma}$, and taking the two anterior items of the Taylor expansion of $\dot{\varepsilon}^{\mathrm{c}}(\boldsymbol{\sigma} + d\boldsymbol{\sigma})$, we get

$$\dot{\boldsymbol{\varepsilon}}_{i+1}^{\mathrm{c}} = \dot{\boldsymbol{\varepsilon}}_i^{\mathrm{c}} + \left.\frac{\partial\dot{\boldsymbol{\varepsilon}}^{\mathrm{c}}}{\partial\boldsymbol{\sigma}}\right|_i \Delta\boldsymbol{\sigma}_i = \dot{\boldsymbol{\varepsilon}}_i^{\mathrm{c}} + \mathbf{H}_i\Delta\boldsymbol{\sigma}_i$$

where

$$\mathbf{H}_i = \left.\frac{\partial\dot{\boldsymbol{\varepsilon}}^{\mathrm{c}}}{\partial\boldsymbol{\sigma}}\right|_i$$

This matrix can be computed from viscoplastic constitutive relation:

$$\dot{\boldsymbol{\varepsilon}}^{\mathrm{c}} = \dot{\overline{\varepsilon}}^{\mathrm{c}}(\partial F/\partial\boldsymbol{\sigma}) = \dot{\overline{\varepsilon}}^{\mathrm{c}}(\partial\overline{\sigma}/\partial\boldsymbol{\sigma})$$

Then

$$\Delta\boldsymbol{\varepsilon}_i^{\mathrm{c}} = \dot{\boldsymbol{\varepsilon}}_i^{\mathrm{c}}\Delta t_i + \theta\Delta t_i\mathbf{H}_i\boldsymbol{\sigma}_i \tag{1.151}$$

1. The viscoelastic constitutive equation
   Substituting Equations 1.150 and 1.151 into the elastic constitutive equation and supposing

   $$\Delta\boldsymbol{\varepsilon}^{\mathrm{p}} = \mathbf{0}$$

   we obtain

   $$\Delta\boldsymbol{\sigma}_i = \hat{\mathbf{C}}^{\mathrm{e}}\left(\Delta\boldsymbol{\varepsilon}_i - \Delta\boldsymbol{\varepsilon}_i^{\mathrm{T}} - \dot{\boldsymbol{\varepsilon}}_i^{\mathrm{e}}\Delta t_i\right)$$

   where

   $$\hat{\mathbf{C}}^{\mathrm{e}} = \left[(\mathbf{C}^{\mathrm{e}})^{-1} + \theta\mathbf{H}_i\Delta t_i\right]^{-1}$$

2. The viscoplastic constitutive equation
   Expressing $\Delta\boldsymbol{\varepsilon}^{\mathrm{p}}$ by the flow rule and adding it to the viscoelastic constitutive equation, we get

$$\Delta\boldsymbol{\sigma}_i = \hat{\mathbf{C}}^{\mathrm{ep}}(\Delta\boldsymbol{\varepsilon}_i - \Delta\boldsymbol{\varepsilon}_i^{\mathrm{T}} - \dot{\boldsymbol{\varepsilon}}_i^{\mathrm{e}}\Delta t_i) + \Delta\overline{\boldsymbol{\sigma}}_i^{\mathrm{T}} \tag{1.152}$$

   where

$$\hat{\mathbf{C}}^{\mathrm{ep}} = \hat{\mathbf{C}}^{\mathrm{e}} - \hat{\mathbf{C}}^{\mathrm{p}}$$

$$\hat{\mathbf{C}}^{\mathrm{p}} = \frac{\hat{\mathbf{C}}^{\mathrm{e}}\frac{\partial F}{\partial\boldsymbol{\sigma}}\left(\frac{\partial F}{\partial\boldsymbol{\sigma}}\right)^{\mathrm{T}}\hat{\mathbf{C}}^{\mathrm{e}}}{H + \left(\frac{\partial F}{\partial\boldsymbol{\sigma}}\right)^{\mathrm{T}}\hat{\mathbf{C}}^{\mathrm{e}}\frac{\partial F}{\partial\boldsymbol{\sigma}}}$$

   $\Delta\overline{\boldsymbol{\sigma}}_i^{\mathrm{T}}$ can be referred to in Equation 1.147.

Different types of creep equations are determined by experiment, which vary with different materials and deformation conditions. Some of them, commonly used in engineering computations, are given below.

1. A creep rule in the uniaxial loading [46]

$$\varepsilon_c = A\sigma^n t^m$$

   i.e.,

$$\dot{\varepsilon}_c = mA\sigma^n t^{m-1}$$

   where
   m, n, and A are the material constants [46]
   t is the time

2. Anand model [47]

$$\dot{\overline{\varepsilon}} = A_0(shB\overline{\sigma})^n \mathrm{e}^{\frac{\Omega}{T+273}}$$

   where
   $\overline{\sigma}$ is the equivalent stress
   T is the temperature (°C)
   A_0, B, Ω, and n are the material constants

3. Power law for the second stage creep [48]

$$\dot{\overline{\varepsilon}}^{\mathrm{e}} = k_1\overline{\sigma}^{k_2}\mathrm{e}^{-\frac{k_3}{T}}$$

   where k_1, k_2, and k_3 are the material constants.

1.6 BASICS OF COMPUTATIONAL FLUID DYNAMICS IN THERMAL PROCESSING

1.6.1 Introduction

The flow phenomena are very common during thermal processing and have various forms. For example, the liquid materials fulfill the filling through flowing in the casting and injection forming; the gas flow in the heat treatment furnaces are helpful in ensuring the uniformity of furnace wall and atmosphere; and the quenching media flow is usually critical to improve quenching ability and product quality. In all these engineering problems, the continuum model has been widely adopted, which takes a series of state variables, such as pressure, velocity, density, temperature, and so on, describing the flow as continuous functions of time and spatial coordinates. Hence, the daedal forms of flow during different thermal processes are dominated by the most fundamental physical laws, namely, the mass conservation law, the momentum conservation law, and the energy conservation law.

In this section, the mathematical expressions of different laws, namely, the governing PDEs, in fluid flow and the monodromy conditions (i.e., initial and boundary conditions) making one process different from others, are introduced from the view of fluid mechanics. The fundamental ideas and commonly used numerical methods to solve the governing PDEs are also briefly discussed.

1.6.2 Governing Differential Equations for Fluid

All of computational fluid dynamics (CFD), in one form or another, is based on the fundamental governing equations of fluid dynamics: the continuity, momentum, and energy equations. They are the mathematical statement of three fundamental physical principles upon which all of fluid dynamics is based:

1. Mass is conserved
2. Newton's second law, $\mathbf{F} = \mathbf{ma}$
3. Energy is conserved

1.6.2.1 Generalized Newton's Law

The relationship between stress tensor and strain tensor for the viscous fluid can be described by generalized Newton's law. The constitutive equation is

$$[\tau] = 2\eta[\varepsilon] - (p - \lambda \nabla V)[I] \tag{1.153}$$

where

$[\tau]$ is the stress tensor
η is the dynamic viscosity coefficient
p is the static pressure of fluid
V is the velocity vector
$[I]$ is the unit vector
$[\varepsilon]$ is the strain tensor
λ ($\lambda = -2/3\ \eta$) is the second viscosity coefficient

In the Cartesian space, the strain tensor can be expressed as

$$[\varepsilon] = \begin{bmatrix} \varepsilon_x & \varepsilon_{xy} & \varepsilon_{xz} \\ \varepsilon_{yx} & \varepsilon_y & \varepsilon_{yz} \\ \varepsilon_{zx} & \varepsilon_{zy} & \varepsilon_z \end{bmatrix} = \begin{pmatrix} \dfrac{\partial u}{\partial x} & \dfrac{1}{2}\left(\dfrac{\partial v}{\partial x}+\dfrac{\partial u}{\partial y}\right) & \dfrac{1}{2}\left(\dfrac{\partial u}{\partial z}+\dfrac{\partial w}{\partial x}\right) \\ \dfrac{1}{2}\left(\dfrac{\partial v}{\partial x}+\dfrac{\partial u}{\partial y}\right) & \dfrac{\partial v}{\partial y} & \dfrac{1}{2}\left(\dfrac{\partial w}{\partial y}+\dfrac{\partial v}{\partial z}\right) \\ \dfrac{1}{2}\left(\dfrac{\partial u}{\partial z}+\dfrac{\partial w}{\partial x}\right) & \dfrac{1}{2}\left(\dfrac{\partial w}{\partial y}+\dfrac{\partial v}{\partial z}\right) & \dfrac{\partial w}{\partial z} \end{pmatrix} \tag{1.154}$$

where u, v, and w are the components of V along the coordinates x, y, and z.

The constitutive equation in the Cartesian space can thus be expressed as

$$\begin{cases} \sigma_x = -p + \lambda \nabla \mathbf{v} + 2\eta \dfrac{\partial u}{\partial x} \\ \sigma_y = -p + \lambda \nabla \mathbf{v} + 2\eta \dfrac{\partial v}{\partial y} \\ \sigma_z = -p + \lambda \nabla \mathbf{v} + 2\eta \dfrac{\partial w}{\partial z} \\ \tau_{xy} = \tau_{yx} = \eta\left(\dfrac{\partial u}{\partial y}+\dfrac{\partial v}{\partial x}\right) \\ \tau_{zx} = \tau_{xz} = \eta\left(\dfrac{\partial u}{\partial z}+\dfrac{\partial w}{\partial x}\right) \\ \tau_{yz} = \tau_{zy} = \eta\left(\dfrac{\partial v}{\partial z}+\dfrac{\partial w}{\partial y}\right) \end{cases} \tag{1.155}$$

where

σ_x, σ_y, and σ_z are the normal stress

τ_x, τ_y, and τ_z are the shear stress

1.6.2.2 Continuity Equation (Mass Conservation Equation)

The fundamental physical principle that mass is conserved means that net mass flow out of the infinitesimal fluid element through surface equals the time rate of decrease in mass inside the infinitesimal fluid element. Hence, the continuity equation can be derived as

$$\frac{\partial \rho}{\partial t} + \nabla(\rho \mathbf{v}) = 0 \tag{1.156}$$

In the Cartesian space, it becomes

$$\frac{\partial \rho}{\partial t} + \frac{\partial(\rho u)}{\partial x} + \frac{\partial(\rho v)}{\partial y} + \frac{\partial(\rho w)}{\partial z} = 0 \tag{1.157}$$

where

ρ is the fluid

t is the time

$\partial\rho/\partial t$ is the time rate of increase in mass inside the element volume

$((\partial(\rho u)/\partial x) + (\partial(\rho v)/\partial y) + (\partial(\rho w)/\partial z))$ is the time rate of net mass flow out of the element volume

1.6.2.3 Momentum Conservation Equation

Applying another fundamental physical principle to a model of the flow, namely,

Physical principle: $\mathbf{F} = \mathbf{ma}$ (Newton's second law)

The conclusion that the time rate of flow momentum equals the sum of external force acting on it can be arrived at. Therefore, we have the momentum equation:

$$\frac{\rho \mathrm{d}\mathbf{V}}{\mathrm{d}t} = \rho\mathbf{F} + \nabla[\tau] \tag{1.158}$$

where $\mathbf{F}$ is the body force of flow of unit volume.

Substituting Equation 1.153 into Equation 1.158, and writing in the Cartesian space, the expanded form of the momentum equation can be obtained.

$$\begin{cases} \rho\left(\dfrac{\partial u}{\partial t}+u\dfrac{\partial u}{\partial x}+v\dfrac{\partial u}{\partial y}+w\dfrac{\partial u}{\partial z}\right)=\rho F_x-\dfrac{\partial(p-\lambda\nabla\mathbf{V})}{\partial x}+\dfrac{\partial}{\partial x}\left(2\eta\dfrac{\partial u}{\partial x}\right)+\dfrac{\partial}{\partial y}\left[\eta\left(\dfrac{\partial v}{\partial x}+\dfrac{\partial u}{\partial y}\right)\right]+\dfrac{\partial}{\partial z}\left[\eta\left(\dfrac{\partial u}{\partial z}+\dfrac{\partial w}{\partial x}\right)\right] \\ \rho\left(\dfrac{\partial v}{\partial t}+u\dfrac{\partial v}{\partial x}+v\dfrac{\partial v}{\partial y}+w\dfrac{\partial v}{\partial z}\right)=\rho F_y-\dfrac{\partial(p-\lambda\nabla\mathbf{V})}{\partial y}+\dfrac{\partial}{\partial y}\left(2\eta\dfrac{\partial v}{\partial y}\right)+\dfrac{\partial}{\partial x}\left[\eta\left(\dfrac{\partial v}{\partial x}+\dfrac{\partial u}{\partial y}\right)\right]+\dfrac{\partial}{\partial z}\left[\eta\left(\dfrac{\partial v}{\partial z}+\dfrac{\partial w}{\partial y}\right)\right] \\ \rho\left(\dfrac{\partial w}{\partial t}+u\dfrac{\partial w}{\partial x}+v\dfrac{\partial w}{\partial y}+w\dfrac{\partial w}{\partial z}\right)=\rho F_z-\dfrac{\partial(p-\lambda\nabla\mathbf{V})}{\partial z}+\dfrac{\partial}{\partial z}\left(2\eta\dfrac{\partial w}{\partial z}\right)+\dfrac{\partial}{\partial x}\left[\eta\left(\dfrac{\partial u}{\partial z}+\dfrac{\partial w}{\partial x}\right)\right]+\dfrac{\partial}{\partial y}\left[\eta\left(\dfrac{\partial v}{\partial z}+\dfrac{\partial w}{\partial y}\right)\right] \end{cases} \tag{1.159}$$

Equation 1.159 is also called Navier–Stokes equation. The left-hand side of Equation 1.159 is the inertia force, while on the right-hand side of Equation 1.159, the first item is the mass force, the second item is the pressure difference, the third item is the viscous expansion force, and the fourth and fifth items are the viscous deformation force. The third to fifth items are only related to the viscous coefficient and strain tensor.

1.6.2.4 Energy Conservation Equation

According to the first law of thermodynamics, the energy equation can be written as

$$\rho c_p \frac{\mathrm{d}T}{\mathrm{d}t} = -p(\nabla\mathbf{V}) + \nabla(k\nabla T) + \rho q + \Phi \tag{1.160}$$

where

c_p is the specific heat at constant pressure
T is the flow temperature
q is the heat flux in the flow with unit mass
k is the thermal conductivity of the flow

The left-hand side of Equation 1.160 is the increase in system internal energy. On the right-hand side of Equation 1.160, the first item is the work done by the volume change of flow (it equals zero for the incompressible flow), the second item is the energy input by the thermal conduction, the third item is the energy generated by the internal heat source, and the fourth item is the viscous dissipation work, which can be expressed as

$$\Phi = \eta\left[2\left(\frac{\partial u}{\partial x}\right)^2+2\left(\frac{\partial v}{\partial y}\right)^2+2\left(\frac{\partial w}{\partial z}\right)^2+\left(\frac{\partial v}{\partial x}+\frac{\partial u}{\partial y}\right)^2+\left(\frac{\partial w}{\partial y}+\frac{\partial v}{\partial z}\right)^2+\left(\frac{\partial w}{\partial x}+\frac{\partial u}{\partial z}\right)^2\right]+\lambda(\nabla\cdot\mathbf{V})^2 \tag{1.161}$$

Then,

$$\rho c_p\left(\frac{\partial T}{\partial t}+u\frac{\partial T}{\partial x}+v\frac{\partial T}{\partial y}+w\frac{\partial T}{\partial z}\right)=(-p+\lambda\nabla\cdot\mathbf{V})\left(\frac{\partial u}{\partial x}+\frac{\partial v}{\partial y}+\frac{\partial w}{\partial z}\right)$$
$$+\ \eta\left[2\left(\frac{\partial u}{\partial x}\right)^2+2\left(\frac{\partial v}{\partial y}\right)^2+2\left(\frac{\partial w}{\partial z}\right)^2+\left(\frac{\partial v}{\partial x}+\frac{\partial u}{\partial y}\right)^2+\left(\frac{\partial w}{\partial y}+\frac{\partial v}{\partial z}\right)^2+\left(\frac{\partial w}{\partial x}+\frac{\partial u}{\partial z}\right)^2\right]$$
$$+\ \frac{\partial}{\partial x}\left(k\frac{\partial T}{\partial x}\right)+\frac{\partial}{\partial y}\left(k\frac{\partial T}{\partial y}\right)+\frac{\partial}{\partial z}\left(k\frac{\partial T}{\partial z}\right)+\rho q \tag{1.162}$$

1.6.3 General Form of Governing Equations

For the viscous Newtonian fluid, the governing equations of the main state variables that need to be solved in fluid flow problems can be expressed in a generalized form as [49]

$$\frac{\partial}{\partial t}(\rho\Phi)+\frac{\partial}{\partial x_j}(\rho u_j\Phi)=\frac{\partial}{\partial x_j}\left(\Gamma_\Phi\frac{\partial\Phi}{\partial x_j}\right)+S_\Phi \tag{1.163}$$

where

$j=1, 2, 3$, x_j is the coordinate components
u_j is the velocity components along x_j
Φ is the general variable
Γ_Φ is the transmission coefficient
S_Φ is the source item

For the incompressible turbulent flow, the coefficient and source in the equations of CFD model are listed in Table 1.4.

Since there are usually three forms of heat transfer, conduction, convection, and radiation, it is worth mentioning that the control equation discussed here can describe the conduction and convection, but for the radiative flow media, the radiation heat transfer with the furnace wall or among themselves should be considered additionally. The numerical calculation of radiation heat transfer can be found in the related literature [50,51].

1.6.4 Simplified and Special Equations in Thermal Processing

The basic equations described here are applicable in an unsteady viscous Newtonian fluid, while their solving is extraordinarily complicated. In the modeling of thermal processing, reasonable hypotheses are usually adopted to simplify the governing equations. Some examples are given in Table 1.4.

TABLE 1.4
Coefficients and Source Item in the Generalized Differential Transmission Equation

Equation	Φ	Γ_Φ	S_Φ
Continuity equation	1	0	0
Momentum equation	u_j	0	$\rho g_i-\frac{\partial p}{\partial x_i}+\eta\nabla^2 u_i$
Energy equation	T	$\frac{K}{c_p}$	$\eta\left[2\left(\frac{\partial u_i}{\partial x_i}\right)^2+\left(\frac{\partial v}{\partial x}+\frac{\partial u}{\partial y}\right)^2+\left(\frac{\partial w}{\partial y}+\frac{\partial v}{\partial z}\right)^2+\left(\frac{\partial w}{\partial x}+\frac{\partial u}{\partial z}\right)^2\right]+\lambda(\nabla\mathbf{V})^2+\rho q$

1.6.4.1 Continuity Equation for Incompressible Source-Free Flow

The incompressible source-free flow, for example, the filling process during casting, has a null divergence of flow velocity at any point in the domain filled with flow; i.e., there is no source and leaking of flow. It follows the mass conservation law. Therefore, the continuity equation can be simplified as follows:

$$\frac{\partial u}{\partial x}+\frac{\partial v}{\partial y}+\frac{\partial w}{\partial z}=0 \tag{1.164}$$

1.6.4.2 Euler Equations for Ideal Flow

For the ideal flow without viscous force, the forces acting on the infinitesimal cubic element include the gravity and pressure upon six surfaces. According to Newton's second law, we have

$$\begin{cases}(\mathrm{d}x\ \mathrm{d}y\ \mathrm{d}z)\rho g_x-\mathrm{d}p(\mathrm{d}y\ \mathrm{d}z)=(\mathrm{d}x\ \mathrm{d}y\ \mathrm{d}z)\rho a_x\\(\mathrm{d}x\ \mathrm{d}y\ \mathrm{d}z)\rho g_y-\mathrm{d}p(\mathrm{d}z\ \mathrm{d}x)=(\mathrm{d}x\ \mathrm{d}y\ \mathrm{d}z)\rho a_y\\(\mathrm{d}x\ \mathrm{d}y\ \mathrm{d}z)\rho g_z-\mathrm{d}p(\mathrm{d}x\ \mathrm{d}y)=(\mathrm{d}x\ \mathrm{d}y\ \mathrm{d}z)\rho a_z\end{cases} \tag{1.165}$$

where a_x, a_y, and a_z are the three components of acceleration, and they are the derivatives of three velocity components, respectively. That is,

$$a_x=\frac{\mathrm{d}u}{\mathrm{d}t},\quad a_y=\frac{\mathrm{d}v}{\mathrm{d}t},\quad a_z=\frac{\mathrm{d}w}{\mathrm{d}t}$$

The acceleration here means the velocity change in the motion of an infinitesimal fluid element, instead of that of the different flow passing through a certain position. The former is the substantial derivative of velocity to time and spatial coordinates while the latter is the partial derivative to time only, and their relationship is

$$\begin{cases}\dfrac{\mathrm{d}u}{\mathrm{d}t}=\dfrac{\partial u}{\partial t}+\dfrac{\partial u}{\partial x}\dfrac{\partial x}{\partial t}+\dfrac{\partial u}{\partial y}\dfrac{\partial y}{\partial t}+\dfrac{\partial u}{\partial z}\dfrac{\partial z}{\partial t}\\[2ex]\dfrac{\mathrm{d}v}{\mathrm{d}t}=\dfrac{\partial v}{\partial t}+\dfrac{\partial v}{\partial x}\dfrac{\partial x}{\partial t}+\dfrac{\partial v}{\partial y}\dfrac{\partial y}{\partial t}+\dfrac{\partial v}{\partial z}\dfrac{\partial z}{\partial t}\\[2ex]\dfrac{\mathrm{d}w}{\mathrm{d}t}=\dfrac{\partial w}{\partial t}+\dfrac{\partial w}{\partial x}\dfrac{\partial x}{\partial t}+\dfrac{\partial w}{\partial y}\dfrac{\partial y}{\partial t}+\dfrac{\partial w}{\partial z}\dfrac{\partial z}{\partial t}\end{cases} \tag{1.166}$$

Substituting Equation 1.166 into Equation 1.167, the momentum equation for the ideal flow, namely, Eular equation, can be obtained as

$$\begin{cases}\rho\left(\dfrac{\partial u}{\partial t}+u\dfrac{\partial u}{\partial x}+v\dfrac{\partial u}{\partial y}+w\dfrac{\partial u}{\partial z}\right)=-\frac{\partial p}{\partial x}+\rho g_x\\[2ex]\rho\left(\dfrac{\partial v}{\partial t}+u\dfrac{\partial v}{\partial x}+v\dfrac{\partial v}{\partial y}+w\dfrac{\partial v}{\partial z}\right)=-\dfrac{\partial p}{\partial y}+\rho g_y\\[2ex]\rho\left(\dfrac{\partial w}{\partial t}+u\dfrac{\partial w}{\partial x}+v\dfrac{\partial w}{\partial y}+w\dfrac{\partial w}{\partial z}\right)=-\dfrac{\partial p}{\partial z}+\rho g_z\end{cases} \tag{1.167}$$

1.6.4.3 Volume Function Equation

In the simulation of the filling process during casting, the solution algorithm–volume of fluid (SOLA–VOF) method has been developed to determine the position of the free surface [52–57]. It describes the whole flow domain by volume function F, which is defined as

$$F = \text{The volume of flow in an element/element volume}$$

Hence, solving the volume function equation, which can be expressed as follows, provides the state of each element.

$$\frac{\partial F}{\partial t} + \frac{\partial (Fu)}{\partial x} + \frac{\partial (Fv)}{\partial y} + \frac{\partial (Fw)}{\partial z} = 0 \tag{1.168}$$

The value of volume function ranges from 0 to 1. When it equals zero, the element is empty without flow; when it equals unit, the element is full; In other cases, namely, $0 < F < 1$, it means that the element is a surface element, which has flow inside but not fully filled.

Hence, only when the value of volume function has been calculated for each element can the filling and flowing state be obtained for the cast parts at any time.

1.6.5 Numerical Solution of Governing PDEs

The governing PDEs discussed above are applicable to flow and heat transfer processes of all the Newtonian fluid, and the difference between different processes is prescribed by the initial and boundary conditions (generally called monodromy conditions). The combination of governing PDEs and corresponding initial and boundary conditions constitutes the complete mathematical formulation of a physical process.

The initial conditions refer to the spatial distribution of the solving variables at the starting moment of the analysis, and they need to be set initially. However, it is not necessary for the steady problem. The boundary conditions are the evolution of the solving variables or their first derivatives around the domain boundary with the time and position.

Usually, the governing PDEs can be divided into three classes, hyperbolic, parabolic, and elliptic. If PDEs in the whole solving domain belong to the same class, the physical problem can be called after the class of the PDE. Some physical problems, in which there are different classes of PDEs in one solving domain, are the so-called hybrid problems. The main difference in different PDE classes lies on their domain of dependence and domain of influence, which affect their solving methods and strategies in turn.

For the PDEs mentioned here, describing the fluid flow and heat transfer, many mathematical methods have been developed to obtain the analytical solution, which are continuous on the whole solving domain. Up to now, these analytical solutions are subjected only to a few simple cases. The numerical methods have been applied more and more in mass flow and heat transfer problems of practical engineering significance.

The fundamental idea of CFD is first, to replace the field of certain physical variables (velocity field, temperature field, etc.) that are continuous in the spatial and time coordinates with the collection of the values on a series of finite discretized points (nodes); then, to establish the algebraic equation (discretization equation) reflecting the relationship of the values on these discretized nodes based on certain principles; finally, to solve the established algebraic equation to obtain the approximation value of the solving variables. The corresponding flow chart is shown in Figure 1.14.

In the past several decades, many numerical methods have been developed, and their main differences lie in their discretization method of domains and equations, and the algorithm of solving

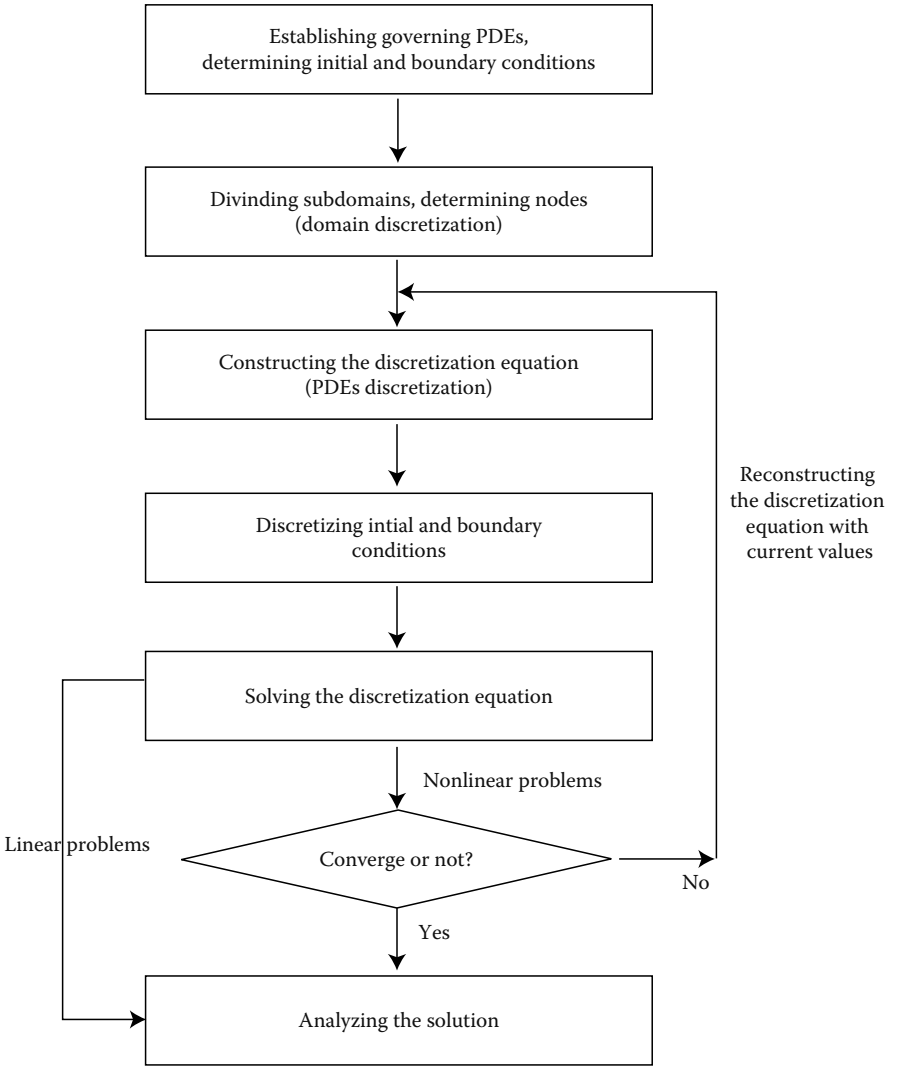

FIGURE 1.14 Flow chart of numerical solving for physical problems.

the algebraic equations. The frequently used methods in CFD are FDM, FEM, finite-volume method (FVM), and finite-analytic method (FAM). The FDM and FEM have been introduced in the previous parts of this chapter; while the FVM and FAM will not be expanded due to space limit; the related studies [58–63] can be referred. In general sense, FVM has obvious superiority over other methods in CFD through the comprehensive evaluation from the view of the ease of implementation, the maturity of development and application, etc.

REFERENCES

1. Segerlind, L.J., *Applied Finite Element Analysis*, 2nd ed., New York: Wiley, 1984.
2. Wait, R. and Mitchell, A.R., *Finite Element Analysis and Applications*, New York: Wiley, 1985.
3. Zienkiewicz, O.C. and Taylor, R.L., *The Finite Element Method*, Vol. 2., New York: McGraw-Hill, 1991.
4. Stasa, F.L., *Applied Element Analysis for Engineers*, New York: Holt, Rinehart, & Winston, 1985.

5. Huebner, K.H. and Thornton, E.A., *The Finite Element Method for Engineers*, 2nd ed., New York: John Wiley & Sons, 1982.
6. Incropera, F.P. and DeWitt, D.P., *Introduction to Heat Transfer*, 3rd ed., New York: John Wiley & Sons, 1996.
7. Reddy, J.N. and Gartling, D.K., *The Finite Element Method in Heat Transfer and Fluid Dynamics*, New York: CRC Press, 2000.
8. Johnson, A.W. and Mehl, R.F., Reactions of kinetics in processes of nucleation and growth, *Transactions AIME*, 1939, 135:416–458.
9. Fernandes, F.M.B., Denis, S., and Simon, A., Mathematical model coupling phased transformation and temperature evolution during quenching of steels, *Materials Science and Technology*, 1985, 1(10):838–844.
10. Avrami, M., *Journal of Chemical Physics*, 1939, 7:1103–1112.
11. Hsu Tsuyao (Xu Zuyao), *Principles of Phase Transformation*, Beijing: Science Press, 1988, pp. 408–419 (in Chinese).
12. Hawbolt, E.B., Chau, B., and Brimacombe, J.K., Kinetics of austenite-ferrite and austenite-pearlite transformation in a 1025 carbon steel, *Metallurgical Transactions A*, 1985, 16A:565–577.
13. Reti, T. and Felde, I., A non-linear extension of the additivity rule, *Computational Materials Science*, 1999, 15:466–482.
14. Tian Dong. Simulation and technology design of quenching of steel workpieces with complex shapes, PhD thesis, Shanghai Jiao Tong University, Shanghai, 1998.
15. Wang, K.F., Chandrasekar, S., and Yang, H.T.Y., Experimental and computational study of the quenching of carbon steel, *Steel Research*, 1996, 67(7):257–265.
16. Pan Jiansheng, Zhang Weimin, Yuan Wenqing, Hu Mingjuan, and Gu Jianfeng, Discussions on the factors affecting the accuracy of computer simulation on heat treatment. *The Proceedings of First Chinese Heat Treatment Week*, 2002, Dalian, pp. 1–11 (in Chinese).
17. Song Dongli, Research of quenching process for large-sized plastic die and mould steel blocks and its application, PhD thesis, Shanghai Jiao Tong University, Shanghai, 2005.
18. Koistinen, D.F. and Marburger, R.E., General equation prescribing the extent of the austenite transformation in pure iron-carbon alloys and plain carbon steels, *Acta Metallurgica*, 1959, 7:50–60.
19. Magee, L.C., Phase transformations, *ASME*., 1970, 115.
20. Hsu Tsuyao (Xu Zuyao), Progress in martensitic transformations (I), *Shanghai Metals*, 2003, 25(3):1–8.
21. Sjöström, S.D. and Simon, A., Coupled temperature, stress, phase transformation calculation model numerical illustration of the internal stresses evolution during cooling of a eutectoid steel cylinder, *Metallurgical Transactions A*, 1987, 18A:1203–1212.
22. Couonna, F., Miassonl, E., Denis, S., et al., On thermo-elastic-viscoplastic analysis of cooling processes including phase changes, *Journal of Materials Processing Technology*, 1992, 34:525–532.
23. Hsu Tsuyao (Xu Zuyao), Progress and perspective of materials heat treatment, *Transaction of Materials and Heat Treatment*, 2003, 24(1):1–13 (in Chinese).
24. Hsu Tsuyao (Xu Zuyao), Fundamentals of the unified technology combining plastic forming and heat treatment of materials, *Engineering Science in China*, 2004, 6(1):16–21 (in Chinese).
25. Denis, S., Archambault, P., Gautier, E., Simon, A., and Beck, G., Prediction of residual stress and distortion of ferrous and non-ferrous metals: Current status and future developments, *Journal of Materials Engineering and Performance*, 2002, 11(1):92–102.
26. Inoue, T. and Wang, Z., Coupling between stress, temperature, metallic structures during processes involving phase transformations, *Materials Science and Technology*, 1985, 1:845–849.
27. Denis, S., Gautier, E., Simon, A., and Beck, G., Stress-phase transformation interactions basic principles, modeling, and calculation of internal stresses, *Materials Science and Technology*, 1985, 1:806–814.
28. Denis, S.P., Archambault, C.A., et al., Modelling of phase transformation kinetics in steels and coupling with heat treatment residual stress production, *Journal of Physics (France)*, 1999(9):323–332.
29. Reese, S., A micromechanically motivated material model for the thermo-viscoelastic material behaviour of rubber-like polymers, *International Journal of Plasticity*, 2003, 19:909–940.
30. Mooney, M., A theory of large elastic deformation, *Journal of Applied Physics*, 1940, 11:582–592.
31. Rivlin, R.S., Large elastic deformations of isotropic materials, *Philosophical Transactions of the Royal Society of London Series A*, 1948, 240:459–490.
32. Rivlin, R.S., Large elastic deformations of isotropic materials. IV. Further developments of the general theory, *Philosophical Transactions of the Royal Society of London Series A*, 1948, 241:379–397.

33. Ogden, R.W., Nonlinear elasticity, anisotropy, material stability and residual stresses in soft tissue, in Holzapfel, G.A. and Ogden, R.W. (Eds.), *Biomechanics of Soft Tissue in Cardiovascular Systems*, Vol. 441, *CISM Courses and Lectures Series*, Wien: Springer, 2003, pp. 65–108.
34. Ogden, R.W., Saccomandi, G., and Sgura, I., Fitting hyperelastic model to experimental data, *Computational Mechanics*, 2004, 34:484–502.
35. Fields D.F. and Backofen, W.A., Determination of strain-hardening characteristics by torsion testing, in *Proceedings of the 60th Annual Meeting of the American Society for Testing and Materials*, Vol. 57, 1957, pp. 1259–1272.
36. Khoddam, S. and Hodgson, P.D., Conversion of the hot torsion test results into flow curve with multiple regimes of hardening, *Journal of Materials Processing Technology,* 2004, 153(special issue):839–845.
37. Chan, K.C. and Gao, L., On the susceptibility to localized necking of defect-free metal sheets under biaxial stretching, *Journal of Materials Processing Technology*, 1996, 58(2–3):251–255.
38. Perzyna, P., Fundamental problems in viscoplasticity, in Kuerti, G. (Ed.), *Advances in Applied Mechanics*, Vol. 9, New York: Academic Press, 1966, pp. 243–377.
39. Lenard, J.G., *Modeling Hot Deformation of Steels*, Berlin: Springer-Verlag, 1989, pp. 101–115.
40. Xing, H.L., Wang, C.W., Zhang, K.F. et al., Recent development in the mechanics of superplasticity and its applications, *Journal of Materials Processing Technology*, 2004, 151(1–3):196–202.
41. Colak, O.U. and Krempl, E., Modeling of uniaxial and biaxial ratcheting behavior of 1026 Carbon steel using the simplified viscoplasticity theory based on overstress (VBO), *Acta Mechanica*, 2003, 160:27–44.
42. Colak, O.U. and Krempl, E., Modeling of the monotonic and cyclic swift effects using an isotropic, finite viscoplasticity theory based on overstress (FVBO), *International Journal of Plasticity*, 2005, 21:573–588.
43. Chaboche, J., Constitutive equations for cyclic plasticity and cyclic viscoplasticity, *International Journal of Plasticity*, 1989, 5:247–302.
44. Hart, E.W., Constitutive relations for the non-elastic deformation of metals, *ASME. Journal of Engineering Material and Technology*, 1976, 98:193–202.
45. Weber, G. and Annand, L., Finite deformation constitutive equations and a time integration procedure for isotropic, hyperelastic–viscoelastic solids, *Computer Methods in Applied Mechanics and Engineering*, 1990, 79:173–202.
46. Miller, A.K., *Unified Constitutive Equations for Creep and Plasticity*, London: Elsevier Applied Science, 1987.
47. Anand, L., Constitutive equations for hot working of metals, *Journal of Plasticity*, 1985, 1:213–231.
48. Frost, H.J. and Ashby, M.F., *Deformation Mechanism Maps: The Plasticity and Creep of Metals and Ceramics*, Oxford: Pergamon Press, 1982.
49. Patankar, S.V., *Numerical Heat Transfer and Fluid Flow*, New York: McGraw-Hill, 1980.
50. Yu Qizheng, *The Principles of Radiation Heat Transfer*, Harbing: Press of Harbing Institute of Technology, 2000, pp. 116–132 (in Chinese).
51. Fan Weicheng and Wan Yuepeng, Models and calculation of flow and combustion, Hefei: University Press of Science and Technology, China, 1992, pp. 202–243 (in Chinese).
52. Hirt, C.W. and Nichols, B.D., Volume of fluid (VOF) method for the dynamics of free boundaries, *Journal of Computational Physics*, 1981, 39:201–225.
53. Stoehr, R.A., Wang, C., Hwang, W.S., and Ingerslev, X., Modeling the filling of complex foundry molds, in Kou, S. and Mehrabian, R. (Eds.), *Modeling and Control of Casting and Welding Process*, 1986, pp. 303–313.
54. Torrey, M.D., Mjolsness, R.C., and Stein, L.R., NASA-VOF3D: A three-dimensional computer program for incompressible flows with free surfaces, Los Alamos National Laboratory Report LA-11009-MS, 1987.
55. Kim, W.-S. and Im, I.-T., Analysis of a mold filling using an implicit SOLA-VOF, *Numerical Heat Transfer. Part A*, 1999, 35(3):1040–7782.
56. Kuo, J.H. and Hwang, W.S., Development of an interactive simulation system for die cavity filling and its application to the operation of a low-pressure casting process, *Modeling and Simulation in Materials Science and Engineering*, 2000, 8(4):583–602.
57. Babaei, R., Abdollahi, J., Homayonifar, P. et al., Improved advection algorithm of computational modeling of free surface flow using structured grids, *Computer Methods in Applied Mechanics and Engineering*, 2006, 195(7–8):775–795.
58. Manole, D.M. and Lage, J.L., Nonuniform grid accuracy test applied to the natural convection flow within a porous medium cavity, *Numerical Heat Transfer*, *Part B*, 1993, 23:351–368.

59. Tan Weiyan, *Computational Shallow Water Dynamics*. Beijing: Tsinghua University Press, 1998 (in Chinese).
60. Tao Wenquan, *Computational Heat Transfer*, Xi'an: Xi'an Jiao Tong University Press, 1988 (in Chinese).
61. Versteeg, H.K. and Malalsekera, W., *An Introduction to Computational Fluid Dynamics*, The Finite Volume Method, Essex: Longman Scientific & Technical, 1995, p. 4.
62. Wei, L.I., *Hybrid Finite Analytic Method for Viscous Flow*, Beijing: Science Press, 2000 (in Chinese).
63. Chen, C.J., Bernatz, R., Carlson, K.D., and Lin, W.L., *Finite Analytic Method in Flows and Heat Transfer*. New York: Taylor & Francis, 2000.

2 Thermodynamics of Thermal Processing

Sivaraman Guruswamy

CONTENTS

2.1 INTRODUCTION

Each milestone in the human history is marked by the development of an ability to produce and manipulate a new material to meet human needs. A wide range of metals and metallic alloys play a key role in our industrialized society. Their importance to our life can be seen from their extensive use in household appliances, ground transportation, power generation/conversion, aerospace, electronics and communication, biological systems, and other applications. Examples of their use are carbon and alloy steels in numerous engineering structures, aluminum alloys in aircraft structures, titanium alloy in the compressor sections of aircraft turbine engines, titanium–aluminum–vanadium alloy used in human orthopedic implants and heart valves, nickel alloys in the combustor sections of aircraft engines, magnesium alloys in space vehicle and satellite components, magnesium alloys for laptop casings, zirconium alloys in nuclear reactor fuel elements, neodymium–iron–boron in high-energy density magnets used in a wide range of high-technology products, and so on. Production of components made of these materials involves various thermal-processing steps. The required properties for each of the applications are obtained through a judicious choice of the principal metallic element, alloying elements, control of the microstructure and thermal or heat treatments. An in-depth understanding of how desirable microstructures in these alloys are obtained through the